NUMERICAL INVESTIGATION OF DBD IN NEON:EFFECT OF FLUID MODELLING APPROACHES

A THESIS SUBMITTED TO
THE GRADUATE SCHOOL OF NATURAL AND APPLIED SCIENCES
OF
MIDDLE EAST TECHNICAL UNIVERSITY

BY

MEHMET HİLMİ SOMAY

IN PARTIAL FULFILLMENT OF THE REQUIREMENTS
FOR
THE DEGREE OF MASTER OF SCIENCE
IN
PHYSICS

FEBRUARY 2021

Approval of the thesis:

NUMERICAL INVESTIGATION OF DBD IN NEON:EFFECT OF FLUID MODELLING APPROACHES

submitted by **MEHMET HİLMİ SOMAY** in partial fulfillment of the requirements for the degree of **Master of Science in Department, Middle East Technical University** by,

Prof. Dr. Halil Kalıpçılar
Dean, Graduate School of **Natural and Applied Sciences** _____

Prof. Dr. Altuğ Özpineci
Head of Department, **Physics** _____

Prof. Dr. İsmail Rafatov
Supervisor, **Physics, METU** _____

Examining Committee Members:

Assoc. Prof. Dr. Serhat Çakır
Physics, METU _____

Prof. Dr. İsmail Rafatov
Phyiscs, METU _____

Assoc. Prof. Dr. Kemal Efe Eseller
Physics, Atılım University _____

Date:11.02.2021

I hereby declare that all information in this document has been obtained and presented in accordance with academic rules and ethical conduct. I also declare that, as required by these rules and conduct, I have fully cited and referenced all material and results that are not original to this work.

Name, Surname: Mehmet Hilmi Somay

Signature :

ABSTRACT

NUMERICAL INVESTIGATION OF DBD IN NEON:EFFECT OF FLUID MODELLING APPROACHES

Somay, Mehmet Hilmi
M.S., Department of Physics
Supervisor: Prof. Dr. İsmail Rafatov

February 2021, 59 pages

The study deals with numerical modelling of dielectric barrier discharge (DBD) in Neon gas. The DBD models are based on the drift-diffusion theory of gas discharges. Two different approaches, namely, the so called simple and extended fluid models, are followed. Within the simple fluid model, the ionization rate is approximated by the Townsend formula as a function of the local electric field. In the framework of the extended fluid model, the electron transport (mobility and diffusion) coefficients as well as the rates of the electron induced plasma-chemical reactions are determined as functions of the electron mean energy. These data are determined from the solution of the electron Boltzmann equation, by using Bolsig+ solver and verified by Comsol Multiphysics package. The electron kinetic coefficients are also computed assuming Maxwellian eedf. Numerical simulations are spatially one-dimensional, carried out using Comsol Multiphysics. The effect of different modelling approaches on the characteristics of DBD is investigated.

Keywords: DBD, Townsend

ÖZ

NEON GAZINDA OLUŞAN DBD NİN NÜMERİK OLARAK ARAŞTIRILMASI: FARKLI AKIŞKAN MODELLERİN ETKİLERİ

Somay, Mehmet Hilmi
Yüksek Lisans, Fizik Bölümü
Tez Yöneticisi: Prof. Dr. İsmail Rafatov

Şubat 2021 , 59 sayfa

Çalışma Neon gazı içerisinde oluşan dielektrik bariyer boşalımının (DBD) nümerik modellemesiyle ilgilidir. DBD modeller gaz boşalımlarının drift-difüzyon teorisine dayanmaktadır. Uygulanan iki yaklaşımdan biri basit diğeri genişletilmiş akışkan modelleridir. Basit akışkan modelinde iyonlaşma hızı yerel elektrik alanının fonksiyonu olarak Townsend formülüne göre hesaplanmıştır. Genişletilmiş akışkan modelinde ise elektron transport (mobilite ve difüzyon) katsayıları ile elektron kaynaklı plasma-kimyasal reaksiyonların hızları ortalama elektron enerjisinin fonksiyonları olarak belirlenmektedir. Bu data Bolsig+ solver kullanılarak elektron Boltzmann denkleminin çözümünden bulunmuş ve Comsol Multiphysics paketini kullanılarak doğrulanmıştır. Elektron kinetik katsayıları ayrıca Maxwell eedf varsayılarak hesaplanmıştır. Uzaysal bir boyutlu nümerik simülasyonlar Comsol Multiphysics kullanılarak sürdülmüştür. Farklı modelleme yaklaşımlarının DBD özelliklerine etkileri araştırılmıştır.

Anahtar Kelimeler: DBD, Townsend

to people i love

ACKNOWLEDGMENTS

There is only one person who affected me at different level and summarize my life perception with their quotes and bare no matter lifes give you. He is George Carlin.Most beautiful one is he mentioned in his comedy that when you are dead ,you don't know that you are dead,it is only difficult for the others,it is same when you are stupid. His many quotes and understanding of life feel me that I am not alone .(Actually this queto is anonymous, because of George Carlin' language i prefer to share this one.)

Especially, I want to thank Prof.Dr. Bayram Tekin for fighting about everything he did. I tried to spend generalize what he did for people as help , but i understood that it is impossible to summarize it here. And also , I wanted to thank Prof.Dr.Osman Yılmaz for being nicest academic person around us.

I want to thank Prof.Dr.İsmail Rafatov for helping me to finish my MSc thesis. He is kind of person that if you ask help from him and he is able to do that, he will do it without giving second thought.

TABLE OF CONTENTS

LIST OF TABLES

TABLES

LIST OF FIGURES

FIGURES

LIST OF ABBREVIATIONS

ABBREVIATIONS

DBD	Dielectric Barrier Discharge
DC	Direct Current
AC	Alternating Current
NTP	Nonthermal Plasmas
PIC	Particle in Cell Method
LFA	Local Field Approximation
LMEA	Local Mean Energy Approximation
MC	Monte Carlo
RF	Radio Frequency
CCD	Charge-coupled Cameras
ICCD	Intensified Charge-coupled Cameras

CHAPTER 1

INTRODUCTION

Plasma word is an ancient word from Ancient Greek which means moldable substance. The plasma first is recognized in Crookes tubes which are invented by Sir William Crookes in 1879. The concept of plasma first is described by Irving Langmuir [1] to state a region of a gas discharge where the number of ions and electrons were equal in 1928. This definition is extended and referring to the collective behaviour of the particles the base on the long range Coulomb interactions [2]. At that point from now on, it was accepted as the fourth state of the matter. Plasma can be the most abundant form of the universe; even though, the phenomena of dark matter has unknown properties. Plasma consists of ionized ions and electrons with neutral species that differ from the gases. One property of plasma is collisional, where the driving plasma frequency is of the order of or smaller than the electron–neutral collision frequency. When the density of positively charged particles and negative ones equal to each other, the quasi-neutrality has occurred.

Even though, it is stated that plasma physics is a difficult, mathematical field, whose the study requires a thorough understanding of electromagnetic theory, we have many applications like plasma etching, plasma cutting and so on.

Formation of ionized species can be achieved in two techniques. One technique is that heating the gases to break the Coulomb barrier . The second technique is that applying electric field high enough. When a plasma is formed by an applied electric field is called gas discharges. We can define plasmas in two categories as nonthermal (cold) and thermal (hot) plasmas. In thermal plasmas the heavy particles and electrons have the same temperature; on the other hand, nonthermal plasmas ions and neutrals have lower temperature compared to electron temperature($T_e > T_n$)

1.1 Classification of Plasmas

Plasmas can be classified following features.

Temperature:

- Low temperature plasmas (T_e< 100 eV)

  In the recent developments in the low-temperature plasmas: Surface hardening of stainless steel as an example of improving material performance with hand of plasma [3]. Working on textiles and fibres [4]. Using charged particles of plasmas to cleaning and protection of the metallic heritage artefacts [5]. Producing anti-bacterial textiles using plasmas [6]. Creating nanocomposite coating and plasma adjustments to wood-based products [7].

- High temperature plasmas (T_e> 100eV)

The highlighted developments in the high-temperature plasmas: Plasma shielding in ITER [11] and Tokamaks [12]. Producing vacuum ultraviolet lasers [13].

Important note that important mathematical difference between high-temperature plasmas and low-temperature plasmas is that we are dealing with $\frac{v}{c}$ terms and $\mathbf{v} \times \mathbf{B}$ term in the Lorentz force [14].

Pressure:

- Low-pressure plasmas (p <10 Torr)

  Surface modifications of plastics such as surface activation (e.g., plasma, corona, flame and UV laser), surface coating (e.g., plasma polymerization, chemical vapour deposition, Parylene, physical vapour deposition) with using low-pressure plasmas [25]. Low pressure plasma spraying for fabricating of the intermetallic matrix composites [28]. Polymer material synthesis and processing with the help of low-pressure plasmas [29].

- Moderate-pressure plasmas(10 Torr < p < 100 Torr)

Important note that there is no clear specification with respect classification of pressure so that some of the low-pressure or high-pressure plasmas can be mentioned in the moderate-pressure plasmas.

- High pressure plasmas(p > 100 Torr)

  The atmospheric plasma jets for creating polymer coatings for biocompatibility and reduced unspecified adsorption [23]. Creating polymeric materials for implant applications with help of atmospheric plasma jets [24]. Ambient air treatment, controlled air treatment, gas precursor coating, liquid precursor coating by using atmospheric plasma [26].

Ionization Degree(α=$n_i/(n_i+n_n)$): n_i is the density of ion n_n is the density of neutral species

- Weakly ionized plasmas ($\alpha < 10^{-3}$)

  Alfven waves in the solar chromosphere, studying ion, ion-neutral collisions in specules, Farley-Buneman instability in chromospheric plasma, Kelvin-Helmholtz instability in solar chromospheric jets [30].

- Fully ionized plasmas($\alpha \sim 1$)

  Industrial applications with using Polycrystalline CVD (Chemical Vapour Deposition) Diamond [31], industrial plasmas which are thermal plasmas and glow discharge plasmas and fusion plasmas have much higher temperatures compare to industrial plasmas [32].

Thermodynamic Equilibrium:

- Nonthermal plasmas ($T_e > T_i$)

  Nonthermal plasmas (NTP) can be applied tissues and living cells for medical applications e.g. wound healing, blood coagulation, sterilization and cancer treatment [8]. Using plasma ability to annhilate bacterial endospores and vegetative cells for achieving food pasteurization[9]. Beside food pasteurization NTP can be also used for microbial decontamination of food products.

- Thermal plasmas($T_i \quad T_e \quad T_n$)

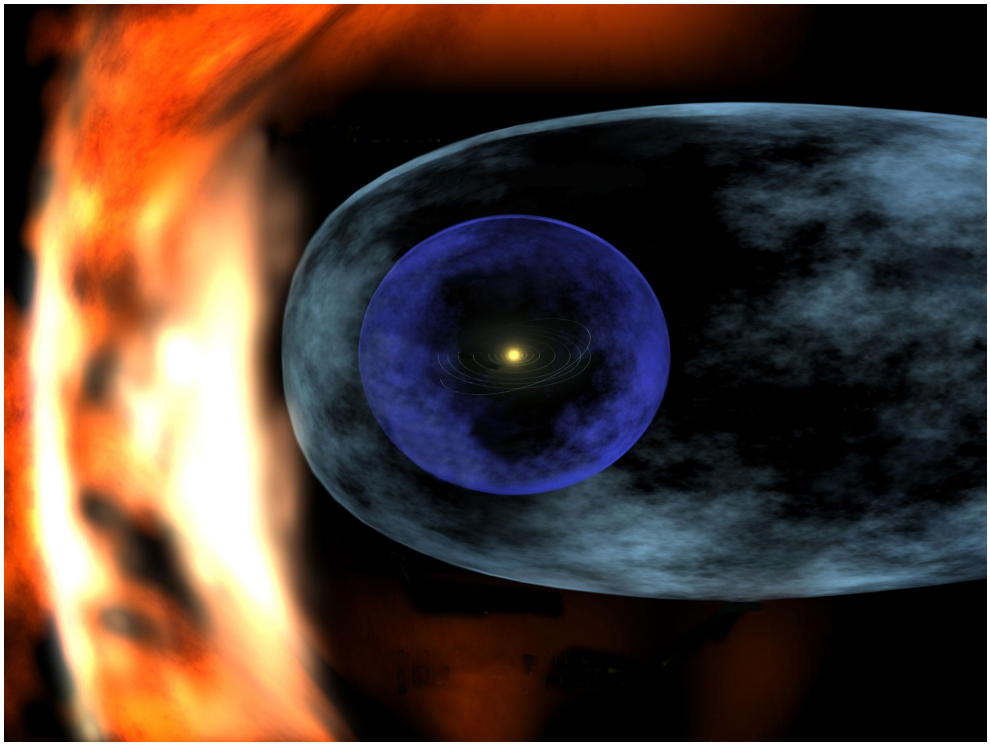

Figure 1.1: The heliosphere [16]

Observing the spectrum of accelerated particles in the heliosphere [15](The solar wind due to Sun, generate a bubble that covers far past the orbits of the Planets). Studying and improving fuel cells. [17]. Planetary magnetospheres are the example of thermal plasmas[18]. Making instruments for planetary exploration missions [19]. High intensity discharge plasmas[20]. Studying spectra of kappa-shaped particles in the planetary magnetospheres [22].

1.2 Glow Discharges

Glow discharges generally occur in an inert gase with applying a voltage that passing striking voltage. In that way, ionization of gas can be self-sustaining and gase start to glow a colour which depends on gase. Beginning of the process, the tube filled with inert gas so that the effects of the cosmic radiation and thermal collisions on the ionization is negligible.

Applying a voltage across the electrode accelerate the free charged species. The

free charged species start to make collisions between neutral atoms. Ionization or excitation are occurred. Due to excitation the electrons jump higher energy level and when it falls back to lower energy state, it emits the characteristic radiation. This is the process responsible for glow in the gase. The accelerated ions hit the electrode walls if ion has more energy than the work function of the surface and then it cause the secondary electron emission. This whole process requires energy so that sustaining the plasma is dependent on the voltage .

Glow discharges have a wide range of applications on the academic world and industrial products. In analytical chemistry, sputtered atoms can be spotted in the gas phase. There is also one method called glow discharge mass spectrometry. These two applications are not widely used because of the limitations of it. Even though the popularity of Plasma TVs is decreased, it is one of the application. Not today but earlier days, zener diode and voltage regulations are accomplished by glow discharge tubes. Sputtering effect of glow discharge tubes are used in the microelectronic industry to manufacture of microelectronics designs. Some of the carbon-dioxide lasers are the application of the glow discharges. Glow discharges also used in surface coating in the thin film industry and academic works. With dielectric barriers glow discharges systems are tested in flow control systems and future investigations are needed.

1.3 Plasma Modelling

Gas discharge physics is a very deep subject and worth to study due to its open questions and industrial significance. Even though it is very promising subject, it required combination of a great deal of knowledge and experience. Experimental setups and numerical simulations are the paths dealing with gas discharge physics. For this purpose Maxwell equations and Boltzmann moments should be coupled with each other, there are very few analytical solutions. (Even if we neglect the chemical reactions in inert gase.) Boltzmann moments are the generalization of Navier-Stokes equations. One of the seven millennium problems is that improving comprehensive understanding on Navier-Stokes equation. When we think about only one problem is solved in 20 years, even if the prize of any solution is one million dollars. For a better understanding of gas discharge physics, it is crystal clear that we need numerical modelling.

Most widely used models are fluid models, kinetic/kinetic-particle and hybrid models.

The kinetic model treats particles as individually. For this purpose, the distribution function is defined as 7-D space $f(\mathbf{r}, \mathbf{v}, t)$. The Boltzmann equation should be solved for the solution of the distribution function. Because of hardship of solving Boltzmann equation, it is needed for some techniques. One of them is two-term approximation. As a particle method, particle in cell method(PIC) govern every single particle according to a fundamental law of physics. Tracking every particle has an enormous amount of computational cost. Answering this problem, Monte Carlo methods are integrated with PIC. Few chemical reactions with a small number of species, low pressure are suitable conditions for PIC method.

Velocity moments of the Boltzmann equation are the root of the fluid model. Three moments ($0^{th}, 1^{st}, 2^{nd}$) are mass, momentum and energy conservation equations respectively. Particle densities, particle velocities, current of species, a charge of species are the possible results of fluid model and there can be more. The fluid approach can be simplified with drift-diffusion approximation. If the transport and reaction rates are calculated by local field this means that LFA approximation is used, if the local mean energy is used this means that LMEA approximation is used.

There is one more option that working the fluid and the kinetic-particle model at the same time which is called a hybrid model. Low energy particle species are governed by fluid equations; on the other hand, fast electrons are solved by MC simulation. Transport coefficients and reaction rates are solved by MC simulation for better precision and accuracy.

1.4 Self-organization and pattern formation in DBD

Pattern formation is the branch of science that is related to the self organization of the system and how pattern is formed in the system. Pattern formation so vast that it is related to many fields like physics, chemistry, mathematics, biology, computer graphics(computer vision problems). Pattern formation for biological systems can be researched with the reaction-diffusion system proposed by Alan Turing in the chemi-

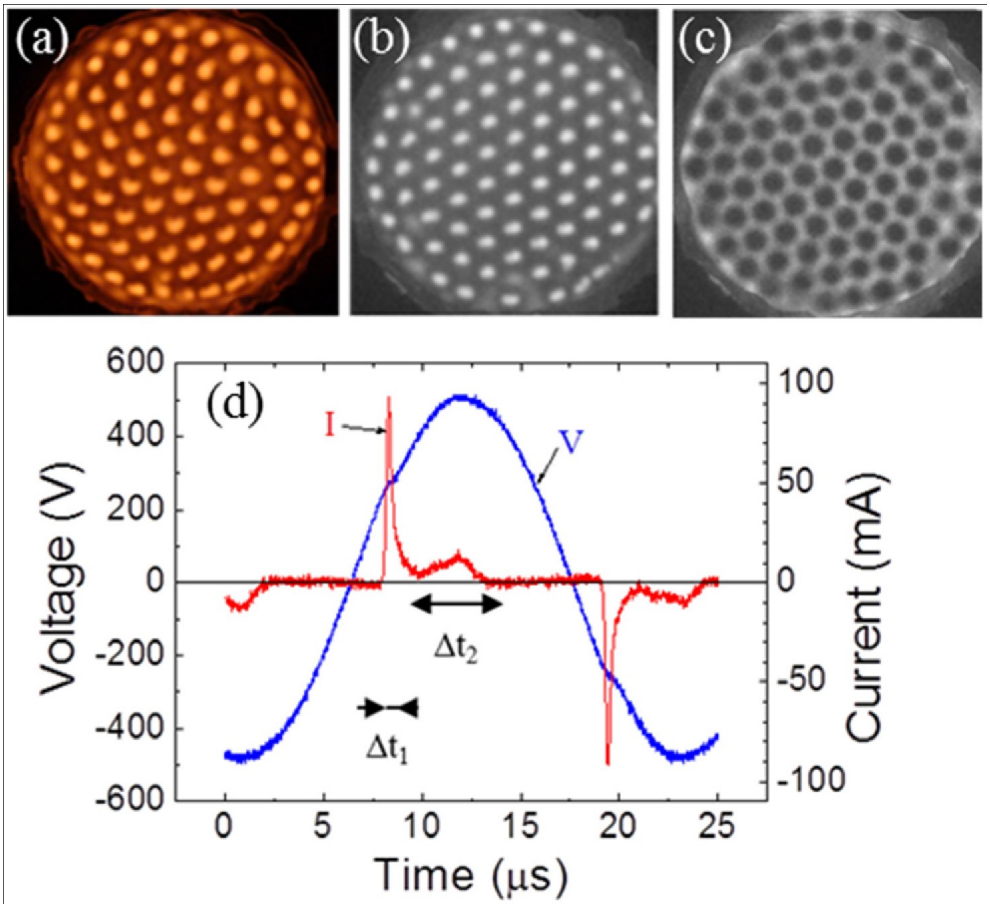

Figure 1.2: The example of pattern formation. In (a) the picture is the discharge of how eyes see, in (b) the image is integrated over the first current pulse, in (c) the image is integrated over the second current pulse, in (d) experimental data in the Ne gase under 100Torr, 500V, 45kHz, gap and dielectric barrier length is 1 mm [36]

.

cal basis of morphogenesis [33].

In this thesis, we deal with the reaction-diffusion system which plasma, surrounded by dielectric barriers, generated by alternating current. When we monitor the filamentary structure, we can observe a self organization system and pattern formation progress. For this purpose, at least two dimensional plasma configuration is required. As it is clear that true understanding of the system is required three dimensional configuration. Mathematical analysis of dielectric barrier discharge systems more fitted to nonlinear systems. On the other hand, we constructed one dimensional model and more dimensional study can provide more promising results.

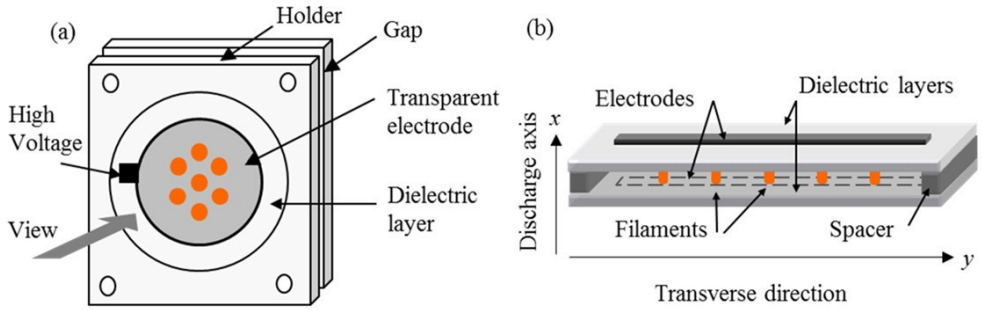

Figure 1.3: Possible DBD configurations from the research group of Laboratoire Plasma et Conversion d'Energie. In (a) configuration , thanks to transparent electrode 2D plasma patterns can be observed, in (b) configuration 1D structures can be observed and the electrodes are linear. Interesting note that the discharge evolution can be easily examined in the configuration (b) not in the configuration (a) [35]

.

According to Paschen curve, we choose correct parameter values that plasma is in the Townsend regime or glow discharge regime. Thanks to that curve we will investigate according to right pressure and voltage values for Townsend breakdown voltage. Other parameters are crucial for study and are taken consideration about them are secondary electron coefficient, alternating current frequency, plasma and dielectric widths.

In DBD systems filamentary behaviour generally observed by charged-coupled cameras (CCD) or intensified charged-coupled cameras (ICCD). The DBD systems have characteristic filamentary discharge or inter-filament dicharge. These filaments can be hexagons, stripes, spiral, concentric rings and so on.

1.5 The aims and objectives of this study

One dimensional the dielectric barrier discharge system form the figure (2.1) is numerically studied. Effect of different electron energy distribution functions (EEDF) are investigated. Simple fluid and extended fluid approaches are used in the models. Two parameter regime (parameter set-1 and parameter set-2 from tables (4.1) and (4.2), two EEDF (Maxwellian and Nonmaxwellian) and two class includes different

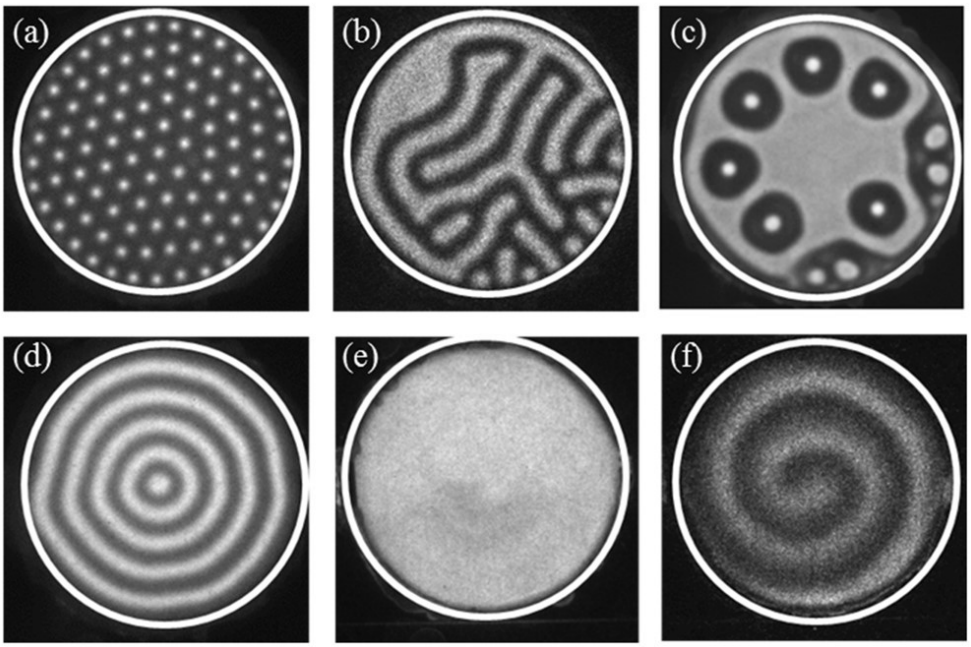

Figure 1.4: (a) Honeycomb shape patterns, (b) and (c) distinct patterns, (d) and (e) spiral patterns, (e) the bright pattern shape [34]

chemical reactions (version 1 is that first eight reactions from table 1 at chapter 2, version 2 is that the all reactions from table 1 in chapter 2) are used to find interesting results. Constructing two and three dimensional models of this study for achieving pattern formation in the DBD system for Ne gas is the future work.

1.6 The Outline of the Thesis

In the first chapter, plasma concept is summarized and what techniques are used in the computational studies. In the second chapter, the fundamentals of the model are described. In chapter three, the Boltzmann equation is introduced and two term approximation is explained. And also, the graphs of transport and reaction rates are showed. In the chapter four, we explained our models and differences. In addition to that our results are visualized. The final chapter is a discussion, we stated our results and findings.

CHAPTER 2

MODELS

We used drift-diffusion approximation to create our models. In the modelling of fluid approach, we followed so called extended fluid and simple fluid approaches. In the models, we also used the Poisson equation for plasma and the Laplace equation for dielectric barriers. We divide our chemical reactions list as two group and we observed the effect of it. Regarding electron energy distribution function, we divide the study into two options as Maxwellian and Nonmaxwellian. And also, we calculated particle transport coefficients and reaction rates via Bolsig+Solver and Comsol Multiphysics Plasma Module. Our study geometry is that 1-dimensional plasma confined by two dielectric barriers.

2.1 Moments of kinetic Boltzmann equation: Derivation of fluid equations for plasma

The Boltzmann equation provides that how $f(\mathbf{r}, \mathbf{v}, t)$ (distribution function) is emerged in time. The Boltzmann equation is applicable under some assumptions. The infinitesimal time interval dt should be long enough to complete the average time duration that any two particle interact so that nearly all interactions are started and completed in dt interval. At the same time, the infinitesimal time interval should be small enough to interact two particle at most once.
Solving the Boltzmann equation is not trivial task. For this reason, we will take integrals over Boltzmann equation for in the information of interest. This approach is called taking the moments of the Boltzmann equation.

Important note that when we further carry out the integrations, we are assuming f is

Maxwell distribution function, will converge to zero rapidly, when $|\mathbf{v}| \to \infty$. In other words, this fact assures that any surface integrals containing f perish over a very large sphere of a radius in velocity space[37]. Maxwell distribution function is isotropic in terms of the velocity vector of the particles and homogeneous in terms of the position of the particles.

Kinetic equation has the form,

$$\frac{\partial f}{\partial t} + (\mathbf{v} \cdot \nabla_{\mathbf{r}}) f + \frac{q}{m}(\mathbf{E} + \mathbf{v} \times \mathbf{B}) \cdot \frac{\partial f}{\partial \mathbf{v}} = \left(\frac{\partial f}{\partial t}\right)_{col.} \tag{2.1}$$

where q is the charge of the particle, m is the mass of the particle, $\mathbf{E}$ is the electric field, $\mathbf{B}$ is the magnetic field, $\nabla_{\mathbf{r}}$ is the gradient in coordinate, f is the distribution function, $\frac{\partial f}{\partial \mathbf{v}}$ is partial derivative respect to velocity; in other words, the gradient in the velocity space, $\left(\frac{\partial f}{\partial t}\right)_{col.}$ is the time rate of change of f because of the collisions.

The Zero Order Moment with the Boltzmann Equation

When we multiply the kinetic equation with v^0 and then integrate it over the velocity space,

$$\begin{aligned} \int \frac{\partial f}{\partial t} d\mathbf{v} + \int (\mathbf{v} \cdot \nabla_{\mathbf{r}}) f d\mathbf{v} \\ + \frac{q}{m} \int [(\mathbf{E} + \mathbf{v} \times \mathbf{B}) \cdot \nabla_{\mathbf{v}}] f d\mathbf{v} = \int \left(\frac{\partial f}{\partial t}\right)_{col.} d\mathbf{v} \end{aligned} \tag{2.2}$$

Under the assumption of the total number of particles are same during the process, the last term of the equation (2.2) can be simplified as

$$\int \left(\frac{\partial f}{\partial t}\right)_{col.} d\mathbf{v} = \left[\frac{\partial}{\partial t} \int f d\mathbf{v}\right] = 0 \tag{2.3}$$

First term of the equation (2.2) can be arranged as

$$\int \frac{\partial f}{\partial t} d\mathbf{v} = \frac{\partial}{\partial t} \int f d\mathbf{v} = \frac{\partial n}{\partial t}, \tag{2.4}$$

where

$$n(\mathbf{r}, t) = \int f(\mathbf{r}, \mathbf{v}, t) d\mathbf{v}. \tag{2.5}$$

$$\mathbf{u}(\mathbf{r},t) = \frac{1}{n(\mathbf{r},t)} \int \mathbf{v} f(\mathbf{r},\mathbf{v},t) d\mathbf{v} \tag{2.6}$$

We can write $\int \mathbf{v} \cdot \nabla_{\mathbf{r}} f d\mathbf{v}$ is equal to $\nabla_{\mathbf{r}} \cdot \int \mathbf{v} f d\mathbf{v}$, because the gradient of the velocity in the position space is zero. This leads to,

$$\int \mathbf{v} \cdot \nabla f d\mathbf{v} = \nabla \cdot (n\mathbf{u}) \tag{2.7}$$

where **u** is the average velocity.

The third term of the equation (2.2) can deduced two separate terms. Starting with **E** part with using Gaussian Theorem in the velocity space,

$$\int \mathbf{E} \cdot \nabla_{\mathbf{v}} f d\mathbf{v} = \int \nabla_{\mathbf{v}} \cdot (f\mathbf{E}) d\mathbf{v} = \int (f\mathbf{E}) \cdot d\mathbf{S} = 0. \tag{2.8}$$

The f goes zero when **v** goes to infinity that makes the integral result to zero.

B part can be written as,

$$\begin{aligned} \int (\mathbf{v} \times \mathbf{B}) \cdot \nabla_{\mathbf{v}} f d\mathbf{v} &= \int \nabla_{\mathbf{v}} \cdot (f\mathbf{v} \times \mathbf{B}) d\mathbf{v} - \int f \nabla_{\mathbf{v}} \cdot (\mathbf{v} \times \mathbf{B}) d\mathbf{v} \\ &= \int f(\mathbf{v} \times \mathbf{B}) \cdot d\mathbf{S} - \int f \nabla_{\mathbf{v}} \cdot (\mathbf{v} \times \mathbf{B}) d\mathbf{v} = 0 \end{aligned} \tag{2.9}$$

The last term of the equation (2.9) is zero because $\mathbf{v} \times \mathbf{B}$ is perpendicular to $\nabla_{\mathbf{v}}$. The first term is zero because $d\mathbf{S}$ is proportional to v^2 and f goes to zero more quickly than surface integral.

After these manipulations and arrangements, it turns out,

$$\frac{\partial n}{\partial t} + \nabla_{\mathbf{r}} \cdot (n\mathbf{u}) = 0 \tag{2.10}$$

The First Order Moment with the Boltzmann Equation

If we multiply equation (2.1) with mv and integrate over the velocity space, we get the first-order of moment,

$$\begin{aligned} m \int \mathbf{v} \frac{\partial f}{\partial t} d\mathbf{v} + m \int \mathbf{v} (\mathbf{v} \cdot \nabla_{\mathbf{r}}) f d\mathbf{v} \\ + q \int \mathbf{v} [(\mathbf{E} + \mathbf{v} \times \mathbf{B}) \cdot \nabla_{\mathbf{v}}] f d\mathbf{v} = \int m\mathbf{v} \left(\frac{\partial f}{\partial t} \right)_{col.} d\mathbf{v} \end{aligned} \tag{2.11}$$

The right-hand side of the equation (2.11) is the change of the momentum due to collisions. In light of the equation (2.7), the first term can be arranged as

$$m\int \mathbf{v}\frac{\partial f}{\partial t} = m\frac{\partial}{\partial t}\int \mathbf{v}f d\mathbf{v} = m\frac{\partial(n\mathbf{u})}{\partial t} \tag{2.12}$$

We can arrange the third term of equation (2.11) as

$$\begin{aligned}\int \mathbf{v}[\mathbf{E}+(\mathbf{v}\times\mathbf{B})]\cdot\nabla_{\mathbf{v}} f d\mathbf{v} &= \int \nabla_{\mathbf{v}}\cdot[f\mathbf{v}(\mathbf{E}+\mathbf{v}\times\mathbf{B})]d\mathbf{v} \\ -\int f\mathbf{v}\nabla_{\mathbf{v}}\cdot(\mathbf{E}+\mathbf{v}\times\mathbf{B})d\mathbf{v} &- \int f(\mathbf{E}+\mathbf{v}\times\mathbf{B})\cdot\nabla_{\mathbf{v}}\mathbf{v}d\mathbf{v}\end{aligned} \tag{2.13}$$

We used Gaussian theorem in equation (2.8) and showed that integral is zero. For same reason, the first two term of the right side of the equation (2.13) is equal to zero. Therefore we have,

$$q\int \mathbf{v}[\mathbf{E}+\mathbf{v}\times\mathbf{B}]\cdot\frac{\partial f}{\partial \mathbf{v}}d\mathbf{v} = -q\int f(\mathbf{E}+\mathbf{v}\times\mathbf{B})d\mathbf{v} = -qn(\mathbf{E}+\mathbf{u}\times\mathbf{B}). \tag{2.14}$$

Using the fact that the gradient operator of the second term of the equation (2.11) does not depend on the velocity vector, the second term of the equation (2.11) can be written as

$$\int \mathbf{v}(\mathbf{v}\cdot\nabla_{\mathbf{r}})f d\mathbf{v} = \int \nabla_{\mathbf{r}}\cdot(f\mathbf{v}\mathbf{v})d\mathbf{v} = \nabla_{\mathbf{r}}\cdot\int f\mathbf{v}\mathbf{v}d\mathbf{v} \tag{2.15}$$

$$= \nabla_{\mathbf{r}}\cdot\int f\mathbf{v}\mathbf{v}d\mathbf{v} = \nabla_{\mathbf{r}}\cdot(n<\mathbf{v}\mathbf{v}>). \tag{2.16}$$

We can separate $\mathbf{v}$ into $\mathbf{v}=\mathbf{u}+\mathbf{w}$ where $\mathbf{u}$ is the averaged fluid velocity and $\mathbf{w}$ is the thermal velocity so we have

$$\nabla\cdot(n<\mathbf{v}\mathbf{v}>) = \nabla\cdot(n\mathbf{u}\mathbf{u}) + \nabla\cdot(n<\mathbf{w}\mathbf{w}>) + 2\nabla\cdot(n\mathbf{u}<\mathbf{w}>). \tag{2.17}$$

The first term of the right-hand side can be written as,

$$\nabla(n\mathbf{u}\mathbf{u}) = \mathbf{u}\nabla\cdot(n\mathbf{u}) + n(\mathbf{u}\cdot\nabla)\mathbf{u} \tag{2.18}$$

Average thermal velocity is zero ($<\mathbf{w}=0>$) and we have stress tensor also called pressure tensor or dyad,

$$\mathbf{\Psi} = mn<\mathbf{w}\mathbf{w}> = \begin{bmatrix} p_{xx} & p_{xy} & p_{xz} \\ p_{yx} & p_{yy} & p_{yz} \\ p_{zx} & p_{zy} & p_{zz}\end{bmatrix}. \tag{2.19}$$

$\mathbf{\Psi}$ is the measure of the thermal motion in a fluid. When the particles move same steady velocity and $\mathbf{w} = 0$, we would have $\mathbf{\Psi} = 0$. The diagonal elements of this tensor are normal pressure components in Cartesian coordinates. For example, p_{zz} is the force per unit area in the z direction applied on a plane surface in the gas normal to z axis. The off-diagonal terms are shearing stresses, e.g. p_{zy} is the force per unit in the y direction exerted on a plane surface perpendicular to z axis.

When the distribution of random velocities **w** is isotropic, diagonal terms became equal to each other and it equals to scalar pressure.

$$\nabla\Psi = \nabla p, \tag{2.20}$$

$$p = \frac{1}{3}mn < w^2 > . \tag{2.21}$$

The equation (2.11) turns out

$$mn\left(\frac{\partial \mathbf{u}}{\partial t} + (\mathbf{u}\cdot\nabla)\cdot\mathbf{u}\right) = -\nabla p + qn(\mathbf{E} + \mathbf{u}\times\mathbf{B}) + \mathbf{S}_{ij}. \tag{2.22}$$

The Second Order Moment of the Boltzmann Equation

Multiplying the Boltzmann equation by $\frac{1}{2}mv^2$ and integrating over velocity space,

$$\begin{aligned}\frac{m}{2}\int v^2\frac{\partial f}{\partial t}d\mathbf{v} + \frac{m}{2}\int v^2(\mathbf{v}\cdot\nabla_{\mathbf{r}})f d\mathbf{v} + \frac{q}{2}\int v^2[(\mathbf{E}+\mathbf{v}\times\mathbf{B})\cdot\nabla_{\mathbf{v}}]f d\mathbf{v} \\ = \int \frac{m}{2}v^2\left(\frac{\partial f}{\partial t}\right)_{coll} d\mathbf{v}\end{aligned} \tag{2.23}$$

The right-hand side of the equation (2.23) is the rate of the change of the energy density which combination of the rate of the energy loss per volume element due to heat transfer, the gained power from the electric field, the energy change due to collision terms and represented as $\mathbf{S}_{coll}$ [38].

The first term of the equation (2.23) can be arranged as

$$\begin{aligned} &\frac{m}{2}\int v^2\frac{\partial f}{\partial t}d\mathbf{v} \\ &= \frac{m}{2}\left(\frac{\partial}{\partial t}\int v^2 f d\mathbf{v} - \int f\frac{\partial}{\partial t}(v^2)d\mathbf{v}\right) \\ &= \frac{\partial}{\partial t}\left(n\frac{1}{2}m < v^2 >\right) \\ &= \frac{\partial}{\partial t}\left(n\frac{1}{2}mu^2\right) \end{aligned} \tag{2.24}$$

where last term of the right hand side of the equation (2.23) is zero , because v^2 is the independent of t implicitly. The second term is

$$\begin{aligned} &\frac{m}{2}\left(v^2\mathbf{v}\cdot\nabla_{\mathbf{r}} f d\mathbf{v}\right) \\ &= \frac{m}{2}\left[\nabla_{\mathbf{r}}\cdot\left(\int \mathbf{v}v^2 f d\mathbf{v}\right) - \int f\mathbf{v}\cdot\nabla_{\mathbf{r}}v^2 d\mathbf{v} - \int f v^2\nabla_{\mathbf{r}}\cdot\mathbf{v}d\mathbf{v}\right] \\ &= \nabla_{\mathbf{r}}\left(n\frac{1}{2}m < v^2\mathbf{v} >\right) \\ &= \nabla_{\mathbf{r}}\left(n\frac{1}{2}m < u^2\mathbf{u} >\right) \end{aligned} \tag{2.25}$$

where the $\nabla_{\mathbf{r}}\cdot\mathbf{v}$ and $\nabla_{\mathbf{r}}v^2$ terms are zero because velocity and spatial variables are independent . The third term is

$$\begin{aligned} &\frac{q}{2}\int v^2[(\mathbf{E}+\mathbf{v}\times\mathbf{B})\cdot\nabla_{\mathbf{v}}]f d\mathbf{v} = \frac{q}{2}\int\nabla_{\mathbf{v}}\cdot[(\mathbf{E}+\mathbf{v}\times\mathbf{B})v^2 f]d\mathbf{v} \\ &-\frac{q}{2}\int f(\mathbf{E}+\mathbf{v}\times\mathbf{B})\cdot\nabla_{\mathbf{v}}v^2 d\mathbf{v} - \frac{q}{2}\int f v^2\nabla_{\mathbf{v}}\cdot(\mathbf{E}+\mathbf{v}\times\mathbf{B})d\mathbf{v} \\ &= -\frac{q}{2}\int f(\mathbf{E}+\mathbf{v}\times\mathbf{B})\cdot\nabla_{\mathbf{v}}v^2 d\mathbf{v} \\ &= -\frac{q}{2}n\left\langle(\mathbf{E}+\mathbf{v}\times\mathbf{B})\cdot\nabla_{\mathbf{v}}v^2\right\rangle \\ &= -\frac{q}{2}n\left\langle(\mathbf{E}+\mathbf{v}\times\mathbf{B})\cdot\nabla_{\mathbf{v}}(\mathbf{v}\cdot\mathbf{v})\right\rangle \\ &= -qn\left\langle(\mathbf{E}+\mathbf{v}\times\mathbf{B})\cdot(\mathbf{v}.\nabla_{\mathbf{v}})\mathbf{v}\right\rangle \\ &= -qn\left\langle(\mathbf{E}+\mathbf{v}\times\mathbf{B})\cdot\mathbf{v}\right\rangle \\ &= -qn < \mathbf{E}\cdot\mathbf{v} > \\ &= -qn < \mathbf{E}\cdot\mathbf{u} > \end{aligned} \tag{2.26}$$

The first term of right-hand side ($\frac{q}{2}\int\nabla_{\mathbf{v}}\cdot[(\mathbf{E}+\mathbf{v}\times\mathbf{B})v^2 f]d\mathbf{v}$) is zero, because when we arrange the integral according to Gaussian theorem, we will notice that the distribution function is zero at infinite velocity. The third term of the right-hand side

($\frac{q}{2}\int fv^2\nabla_{\mathbf{v}}\cdot(\mathbf{E}+\mathbf{v}\times\mathbf{B})d\mathbf{v}$) is zero because all Lorentz force components are independent of the corresponding velocity term[39]. The energy-conversation equation turns out,

$$\begin{aligned}\frac{\partial}{\partial t}\left[n\frac{1}{2}mu^2\right]+\nabla_{\mathbf{r}}\cdot\left[n\frac{1}{2}m<u^2\mathbf{u}>\right]-nq<\mathbf{E}\cdot\mathbf{u}>&\\ =\frac{m}{2}\int u^2\left(\frac{\partial f}{\partial t}\right)_{coll}d\mathbf{u}&\\ =\mathbf{S}_{coll}&\end{aligned}\tag{2.27}$$

The energy-conservation equation can be another form,

$$\frac{\partial}{\partial t}\left(\frac{1}{2}nm<w^2>\right)+\nabla\cdot\left(\frac{1}{2}nm<w^2>\mathbf{u}\right)+(\mathbf{\Psi}\cdot\nabla)\cdot\mathbf{u}+\nabla\cdot\mathbf{q}=\mathbf{S}_{coll}.\tag{2.28}$$

where $\mathbf{q}$ is the heat flux vector in a unit of Wm^{-2}. In isotropic plasma the pressure tensor $\mathbf{\Psi}$ turns out the scalar pressure p and taking account of the average energy of plasma is $\frac{3}{2}p=\frac{1}{2}nm<\mathbf{ww}>$, $p=nk_BT$ under assumption of f is Maxwell distribution function.

The energy conversation simplifies to

$$\frac{\partial(\frac{3}{2})p}{\partial t}+\nabla\cdot\left(\frac{3}{2}p\mathbf{u}\right)-p\nabla\cdot\mathbf{u}+\nabla\cdot\mathbf{q}=\mathbf{S}_{coll}.\tag{2.29}$$

$\frac{3}{2}p\mathbf{u}$ is the flow of the energy density or fluid velocity in units of Wm^{-2} and $p\nabla\cdot\mathbf{u}$ is the heating or cooling of the fluid in the unit of Wm^{-3} because of compression or expansion. $\mathbf{q}$ is the heat-flux vector (unit of Wm^{-2}). In the case of steady-state, low-pressure discharges and the collisional process is equalled to the macroscopic energy flux, the equation (2.29) will be a much simpler equation (2.30).

$$\nabla\cdot\left(\frac{3}{2}p\mathbf{u}\right)=\mathbf{S}_{coll}\tag{2.30}$$

2.2 Transformation of Fluid Equations to Drift-Diffusion Equations

Set of two-fluid model equations are three moments of the Boltzmann equation and the Maxwell equations. Two-fluid term comes from electrons and ions. According to assumption of isotropic case, dyad turns out the scalar pressure. The maxwell

equations are

$$\nabla \cdot \mathbf{B} = \mu_0 \mathbf{J} + \mu_0 \epsilon_0 \frac{\partial \mathbf{E}}{\partial t}, \tag{2.31}$$

$$\nabla \cdot \mathbf{E} = \frac{\sigma}{\epsilon_0}, \tag{2.32}$$

$$\nabla \cdot \mathbf{B} = 0, \tag{2.33}$$

$$\nabla \times \mathbf{E} + \frac{\partial \mathbf{B}}{\partial t} = 0. \tag{2.34}$$

Two fluid equations (continuity, momentum, energy balance equations respectively) are

$$\frac{\partial n_j}{\partial t} + \nabla \cdot (n_j \mathbf{v}_j) - S_j, \tag{2.35}$$

$$m_j n_j (\frac{\partial \mathbf{v}_j}{\partial t} + (\mathbf{v}_j \cdot \nabla)\mathbf{v}_j) + \nabla p_j + q_j n_j (\mathbf{E} - \mathbf{v} \times \mathbf{B}) - \mathbf{S}_{in} - \mathbf{S}_{en}, \tag{2.36}$$

$$\frac{\partial}{\partial t}(\frac{3}{2} p_j) + \nabla \cdot (\frac{3}{2} p_j \mathbf{v}_j) - p_j \nabla \cdot \mathbf{v}_j + \nabla \mathbf{q}_j - \mathbf{Sc}_j, \tag{2.37}$$

where j can be e for the electrons and i for the ions $\sigma = n_i q_i + n_e q_e$, **J=**$\mathbf{n}_i q_i \mathbf{v}_i + n_e q_e, \mathbf{v}_e$,$\mathbf{S}_j$ is the source term, $\mathbf{S}_{in}$ and $\mathbf{S}_{en}$ are the rate of change of momentum between species, $\mathbf{Sc}_j$ is the source term for energy balance equation.

Under the facts that $m_i >> m_e$, $\mathbf{v}_e >> \mathbf{v}_n$, $\rho_i(\mathbf{v}_i \cdot)\mathbf{v}_i >> \rho_e(\mathbf{v}_e \cdot)\mathbf{v}_e$ and $p_j = n_j k_B T_i$ and we assumed that $\mathbf{B} = 0$ two fluid equations turn out,

$$\frac{\partial n_e}{\partial t} + \nabla \cdot (-\mu_e n_e \mathbf{E} - D_e \nabla n_e) - S_e = 0, \tag{2.38}$$

$$\frac{\partial n_i}{\partial t} + \nabla \cdot (\mu_i n_i \mathbf{E} - D_i \nabla n_i) - S_i = 0. \tag{2.39}$$

Assuming $\mathbf{B} = 0$, the only Poisson equation should be solved from Maxwell equations,

$$-\nabla^2 \Phi = \frac{e}{\epsilon_0}(n_i - n_e). \tag{2.40}$$

2.3 Description of the Extended Fluid Model for DBD is Neon

2.3.1 Plasma species taken into account and corresponding set of reactions

In this work, we study two modelling approaches with two different parameter regimes. In the simple fluid model, only secondary electron emission and direct ionization are accounted into consideration. In the extended fluid models, we use calculated transport and reaction rates as Maxwell and Nonmaxwell options from Bolsig+Solver and investigate differences between them. And also, we divide chemical reactions which are introduced in table 1 to two group for investigating effect of last four reactions. First group consist of first eight reactions, second group consist of all of the reactions in Table 1.

Table 1: Elementary reactions considered in this study. Label Boltz indicates that the reaction rate was calculated from Boltzmann Solver.

Index	Reaction	Type	$\Delta E(eV)$	Constant
1	e+Ne $\longrightarrow$ e+Ne	Elastic collision	0	Boltz.
2	e+Ne $\longleftrightarrow$ e+Ne(1s5)	Excitation	16.2	Boltz.
3	e+Ne $\longleftrightarrow$ e+Ne(1s4)	Excitation	16.67	Boltz.
4	e+Ne $\longleftrightarrow$ e+Ne(1s3)	Excitation	16.72	Boltz.
5	e+Ne $\longleftrightarrow$ e+Ne(1s2)	Excitation	16.85	Boltz.
6	e+Ne $\longleftrightarrow$ e+Ne(2P1)	Excitation	18.38	Boltz.
7	e+Ne $\longleftrightarrow$ e+Ne(3D6)	Excitation	20	Boltz.
8	e+Ne$\longrightarrow$ e+e+Ne^+	Ionization	21.56	Boltz.
9	e+Ne(1s2) $\longrightarrow$ e+e+Ne^+	Ionization	4.945	Boltz.
10	e+Ne(1s3) $\longrightarrow$ e+e+Ne^+	Ionization	4.945	Boltz.
11	e+Ne(1s4) $\longrightarrow$ e+e+Ne^+	Ionization	4.945	Boltz.
12	e+Ne(1s5) $\longrightarrow$ e+e+Ne^+	Ionization	4.945	Boltz.

2.3.2 Equations of Model

Fluid model of glow discharges is a combination of continuity, momentum and energy equation for each plasma species. These equations are coupled with the Poisson or the Laplace equation. Local-mean-energy approximation (LMEA) is used in extended fluid model. And also non-local ionization in the negative glow region and Faraday dark space is taken account in the LMEA and it is ignored in the LFA [42].

An extended fluid model with dielectric barriers can be described as

$$\frac{\partial n_k}{\partial t} + \nabla \cdot \mathbf{\Gamma}_k = S_k, \tag{2.41}$$

$$\mathbf{\Gamma}_k = sgn(q_k)\mu_k n_k \mathbf{E} - D_k \nabla n_k, \tag{2.42}$$

$$\epsilon_0 \nabla \cdot \mathbf{E} = \sum_k q_k n_k \ , \ \mathbf{E} = -\nabla \phi. \tag{2.43}$$

In the dielectric barriers,

$$\epsilon \nabla \cdot \mathbf{E} = 0, \tag{2.44}$$

$$\mathbf{E} = -\nabla\phi. \tag{2.45}$$

n_k represents kth species such as electrons, ions, metastable and resonant atoms etc. $\mathbf{\Gamma}_k$ is the particle flux in plasma according to drift-diffusion approach.

Energy equation in the extended fluid model is

$$\frac{\partial n_\epsilon}{\partial t} + \nabla \cdot \mathbf{\Gamma}_\epsilon = -e\mathbf{\Gamma}_e \cdot \mathbf{E} + \frac{3}{2}\frac{m_e}{m_g}\nu_{ea} n_e k_B (T_e - T_g) - \sum_i \Delta E_i R_i, \tag{2.46}$$

where

$$\mathbf{\Gamma}_\epsilon = -D_\epsilon \nabla n_\epsilon - \mu_\epsilon \mathbf{E} n_\epsilon, \tag{2.47}$$

$$n_\epsilon = n_e \bar{\epsilon}. \tag{2.48}$$

In the equation (2.64) n_ϵ is the electron energy density which equals to $\frac{3}{2} n_e k_B T_e$, $\mathbf{\Gamma}_\epsilon$ is the density of the electron energy flux where $D_\epsilon = \frac{5}{3} D_e$ (the electron energy diffusion coefficient) and $\mu_\epsilon = \frac{5}{3}\mu_e$ (the electron energy mobility).

The first term of right-hand side of the equation (2.64) is that Joule heating or cooling of electrons in the electric field. The second term is the elastic loss where ν_{ea} represents the electron-atomic elastic collision frequency and the last term describes the energy loss in the inelastic collisions.

T_g, T_e is the gas and electron temperature, m is the particle mass. ΔE_j is the energy gain or loss and R_j is the corresponding reaction rate.

2.3.3 Transport Coefficients

Calculations are performed for Neon gase and models consider the list of reactions in Table 1. The first process is an elastic scattering of electrons. The cross-section for this process is used to calculate the effective frequency ν_{ea} , mobility μ_e and diffusion

coefficient D_e,

$$\mu_e = -\frac{1}{n_e}\frac{e}{m_e}\int_0^\infty D_r\sqrt{\epsilon}\frac{\partial}{\partial\epsilon}f_0(\epsilon)d\epsilon, \tag{2.49}$$

$$D_e = \frac{1}{n_e}\int_0^\infty D_r\sqrt{\epsilon}f_0(\epsilon)d\epsilon, \tag{2.50}$$

where $\epsilon = mv^2/2e$ is the electron kinetic energy in eV units and $D_r = 2\epsilon/3m_e\nu_{ea}$ is the space diffusion coefficient, $f_0(\epsilon)$ is the EEDF obtained from the solution of local Boltzmann equation and which is normalized by the expression.

$$\int_0^\infty f_0(\epsilon)\sqrt{\epsilon}d\epsilon = 1. \tag{2.51}$$

$$f_0(\epsilon) = \frac{1}{\sqrt{\pi}}\frac{1}{T_e^{3/2}}\exp(-\frac{\epsilon}{T_e}) \tag{2.52}$$

Energy transport coefficients are calculated as $\mu_\epsilon = (5/3)\mu_e$ and $D_\epsilon = (5/3)D_e$. Electron energy density flux is

$$\mathbf{\Gamma}_\epsilon = \frac{5}{2}k_BT_e\mathbf{\Gamma}_e - \lambda_e\nabla k_BT_e, \tag{2.53}$$

where $\lambda_e = \frac{5}{2}n_eD_e$.

2.3.4 Source Terms

S_k are volume source terms in the particle balance equations where,

$$S_k = \sum_i R_i - \sum_j R_j'. \tag{2.54}$$

In the case of the extended model with all plasma chemistry we have,

$$S_e = S_i = R_8 + R_9 + R_{10} + R_{11} + R_{12} = K_8 n_e n_0 + K_9 n_e n_{m1} + K_{10} n_0 n_{m2} + K_{11} n_0 n_{r1} + K_{12} n_e n_{r2} \tag{2.55}$$

Rate constants of chemical reactions are derived from EEDF, obtained from a solution of Boltzmann kinetic equation with corresponding cross-sections,

$$K_R = \int_0^\infty \sigma_R(\epsilon)\sqrt{\epsilon} f_0(\epsilon) d\epsilon. \tag{2.56}$$

We calculated cross-sections and transport coefficients from solver for EEDF via Comsol Multiphysics and Bolsig+Solver.

2.3.5 Boundary Conditions

Boundary conditions for positive ions at the dielectric walls are given as follows:

$$\hat{\mathbf{n}} \cdot \mathbf{\Gamma}_i = 1/4 v_i n_i + \alpha n_i \mu_i (\hat{\mathbf{n}} \cdot \mathbf{E}) \tag{2.57}$$

where thermal velocity $v_i = \sqrt{8 k_B T_i / \pi m_i}$, $\mathbf{\Gamma}$ is the particle flux and $\hat{\mathbf{n}}$ is the normal vector pointing towards the surface, α is either 0 or 1 depending on positive ion drift direction at the surface.

The boundary conditions for the electrons at the dielectric walls are given as follows:

$$\hat{\mathbf{n}} \cdot \mathbf{\Gamma_e} = 1/4 v_e n_e - \gamma \hat{\mathbf{n}} \cdot \mathbf{\Gamma}_i, \tag{2.58}$$

where γ is the secondary electron emission coefficient.

The boundary condition for electron energy density at the dielectric walls are

$$\hat{\mathbf{n}} \cdot \mathbf{\Gamma}_\epsilon = 1/2 v_e n_\epsilon - 2 k_B T_e \gamma \hat{\mathbf{n}} \cdot \mathbf{\Gamma}_i, \tag{2.59}$$

where k_B is the Boltzmann constant.

Figure 2.1: Basic schematic of DBD system in the study

The boundary conditions for Ne(1s5), Ne(1s4), Ne(1s3), Ne(1s2) are same as shown in the equation(2.79)

$$\hat{\mathbf{n}} \cdot \mathbf{\Gamma} = 1/4vn, \tag{2.60}$$

where v is the thermal velocity and n is the particle density.

We set the sinusoidal voltage at the left end is shown in the figure (2.1) $\phi = Vsin(wt)$, where $w = 2\pi f$, f is the driving frequency, t is the time. The right side of the DBD system is a grounded electrode.
At the dielectric walls,

$$\sigma = (\epsilon_r \epsilon_0 \mathbf{E}_d - \epsilon_0 \mathbf{E}) \cdot \hat{\mathbf{n}}, \tag{2.61}$$

where $\mathbf{E}_d$ is the electric field in the dielectric, $\mathbf{E}$ is the electric field, ϵ_0 is the permittivity of the air, ϵ_r is the relative permittivity of the dielectric [42].

The dielectric wall should satisfy the condition,

$$\frac{\partial \sigma}{\partial t} = \sum_j q_j \mathbf{\Gamma}_j(x,t), \tag{2.62}$$

where j can be i (the ion) or e (the electron) in our study [42].

2.4 Reduction of the extended fluid model to simple fluid model

In the simple fluid model, the source term changes to

$$S_e = S_i = |\mathbf{\Gamma}_e|\alpha - \beta n_i n_e. \tag{2.63}$$

The first term of the equation (2.87) is Townsend coefficient, in other words, the coefficient of ionization by electron impact, the second term is the coefficient of ion-

electron recombination and β is the recombination coefficient. Transport coefficients such as D_i, D_e (diffusion coefficients) and μ_e, μ_i (mobility coefficients) are used as constants. It obeys the Einstein relationship,

$$\frac{D}{\mu} = \frac{k_B T}{m}. \tag{2.64}$$

The energy equation is disregarded in the simple fluid approach. There is no difference between simple fluid and extended fluid approach for solving the Poisson and the Laplace equations and applying boundary conditions on Maxwell equations.

2.4.1 Implementation of the DBD model in COMSOL Multiphysics

We use the plasma module of the Comsol Multiphysics for checking for calculations of transport coefficients and reaction rates which are calculated from Bolsig+Solver. Comsol Multiphysics provide a two-term approximation of Boltzmann equation. As a first step, collision data should be uploaded and specify type reaction (e.g excitation, ionization). Secondly, gas temperature, number particle density and mole fractions of gas should be specified. There are four options for distribution function which are Boltzmann, Maxwellian, Druyveystein and generalized. One can also specify an oscillatory field, electron-electron collisions, secondary electron sharing conditions. Solutions can be obtained as a function of reduced electric field or function of mean energy.

CHAPTER 3

CALCULATION OF THE TRANSPORT AND REACTION RATE COEFFICIENTS FOR ELECTRONS

Extended fluid model transport and reaction rates coefficients are obtained from a solution of the Boltzmann equation for an electron energy distribution function. Two-term approximation method is the conventional way to approach to this kind of calculations.

3.1 Two-term approximation for EEDF

The general form of the Boltzmann equation for electrons in plasma is

$$\frac{\partial f}{\partial t} + \mathbf{v} \cdot \nabla f - \frac{e}{m}\mathbf{E} \cdot \nabla_v f - A = 0, \tag{3.1}$$

where f is the electron energy distribution function (EEDF) in 7-D phase space and C is the rate of EEDF because of collision. Under the assumption of uniform electric field and symmetric EEDF in velocity space, Boltzmann equation in the spherical coordinates is

$$\frac{\partial f}{\partial t} + \mathbf{v}\theta\frac{\partial f}{\partial z} - \frac{e}{m}\mathbf{E}\left(cos\theta\frac{\partial v}{\partial x} + \frac{sin\theta^2}{v} + \frac{\partial f}{\partial cos\theta}\right) - A = 0 \tag{3.2}$$

where v is the magnitude of velocity, z and θ are the coordinates. Two terms approximation cancels the dependency of θ and f is expanded in Legendre polynomials and is reshaped in the light of the first two terms of the expansion. More terms can be used for higher accuracy, but the first two terms give satisfying results except very

rare cases. Two terms approximation can be written as

$$f(v, cos\theta, z, t) = f_0(v, z, t) + f_1(v, z, t)cos\theta, \tag{3.3}$$

where we can express f_0 (isotropic velocity part) and f_1 (anisotropic velocity part),

$$\frac{\partial f_0}{\partial t} + \frac{\gamma}{3}\epsilon^{1/2}\frac{\partial f_1}{\partial z} - \frac{\gamma}{3}\epsilon^{-1/2}\frac{\partial}{\partial \epsilon}(\epsilon E f_1) - A_0 = 0, \tag{3.4}$$

$$\frac{\partial f_1}{\partial t} + \frac{\gamma}{3}\epsilon^{1/2}\frac{\partial f_0}{\partial z} - E\gamma\epsilon^{1/2}\frac{\partial f_0}{\partial \epsilon} = -N\sigma_m\gamma\epsilon^{1/2}f_1. \tag{3.5}$$

Here $\gamma = (2e/m)^{1/2}, \epsilon = (v/\gamma)^2$ is the electron energy, N is the gas density, E is the electric fied, σ_m total momentum cross section.

EEDF obtains the form explicitly,

$$f_0(\epsilon, z, t) = \frac{1}{2\pi\gamma^3}F_0(\epsilon)n(z, t), \tag{3.6}$$

$$f_1(\epsilon, z, t) = \frac{1}{2\pi\gamma^3}F_1(\epsilon)n(z, t). \tag{3.7}$$

Normalization conditions are

$$\int_0^\infty F_0\sqrt{\epsilon}d\epsilon = 1, \tag{3.8}$$

$$\int_0^\infty F_1\sqrt{\epsilon}d\epsilon = 1. \tag{3.9}$$

One of the way to calculate the growth of the electron density is that using exponential temporal growth without space for pulsed Townsend experiments. Rate of the electron density growth which is the net production frequency $\bar{\nu}_i$ is

$$\frac{1}{n_e}\frac{\partial n_e}{\partial t} = \bar{\nu_i} = N\gamma\int_0^\infty \left(\sum_{k=ionizaiton}\sigma_k\right) \times \epsilon F_0 d\epsilon. \tag{3.10}$$

Anisotropic velocity part can be obtained as

$$F_1 = \frac{E}{N}\frac{1}{\tilde{\sigma_m}}\frac{\partial F_0}{\partial \epsilon}, \tag{3.11}$$

where

$$\tilde{\sigma_m} = \sigma_m + \frac{\bar{\nu_i}}{N\gamma\epsilon^{1/2}}. \tag{3.12}$$

After substituting to equation (3.4), it turns out

$$-\frac{\gamma}{3}\frac{\partial}{\partial \epsilon}\left(\left(\frac{E}{N}\right)^2 \frac{\epsilon}{\tilde{\sigma}_m}\frac{\partial F_0}{\partial \epsilon}\right) = \tilde{C}_0 + \tilde{R}, \tag{3.13}$$

where

$$\tilde{R} = -\frac{\bar{\nu_i}}{N}\epsilon^{1/2}F_0, \tag{3.14}$$

$$\tilde{C}_0 = 2\pi\gamma^3\epsilon^{1/2}\frac{C_0}{Nn}. \tag{3.15}$$

Equations (3.4), (3.5)turn out

$$-\frac{\gamma}{3}\frac{\partial}{\partial \epsilon}\left(\left(\frac{E}{N}\right)^2 \frac{\epsilon}{\tilde{\sigma}_m}\frac{\partial F_0}{\partial \epsilon}\right) = \tilde{C}_0 + \tilde{R}, \tag{3.16}$$

$$F_1 = \frac{1}{\sigma_m}\left(\frac{E}{N}\frac{\partial F_0}{\partial \epsilon} + \frac{\alpha}{N}F_0\right). \tag{3.17}$$

Here

$$\alpha = \frac{1}{2D}\left(\mu E - \sqrt{(\mu E)^2 - 4D\bar{\nu_i}}\right), \tag{3.18}$$

$$\tilde{R} = \frac{\alpha}{N}\frac{\gamma}{3}\left(\frac{\epsilon}{\sigma_m}\left(2\frac{E}{N}\frac{\partial F_0}{\partial \epsilon} + \frac{\alpha}{N}F_0\right) + \frac{E}{N}F_0\frac{\partial}{\partial \epsilon}\left(\frac{\epsilon}{\sigma_m}\right)\right). \tag{3.19}$$

Collision term can be divided into two part which are electron-electron and contribution from all different collision processes. In the short, final version of the electron-electron collision term is

$$\tilde{C}_0 = \sum_k \tilde{C}_{0,k} + \tilde{C}_{0,e}, \tag{3.20}$$

$$\tilde{C}_{0,e} = a\frac{n}{N}\frac{\partial}{\partial\epsilon}\left(3A_1F_0 + 2(A_2 + \epsilon^{3/2}A_3)\frac{\partial F_0}{\partial\epsilon}\right). \tag{3.21}$$

Expansion of terms to equation (3.22) is

$$A_1 = \int_0^{\epsilon} u^{1/2}F_0(u)du, \tag{3.22}$$

$$A_2 = \int_0^{\epsilon} u^{3/2}F_0(u)du, \tag{3.23}$$

$$A_3 = \int_0^{\infty} u^{1/2}F_0(u)du, \tag{3.24}$$

$$\Lambda = \frac{12\pi(\epsilon_0 k_B T_e)^{3/2}}{e^3 n^{1/2}}, \tag{3.25}$$

$$a = \frac{e^2\gamma}{24\pi\epsilon_0^3} ln\Lambda, \tag{3.26}$$

$$k_B T_e = \frac{2}{3}eA_2(\infty). \tag{3.27}$$

EEDF can be represented as the stationary convection-diffusion equation,

$$\frac{d}{d\epsilon}\left(\tilde{W}F_0 - \tilde{D}\frac{dF_0}{d\epsilon}\right) = \tilde{S}, \tag{3.28}$$

where

$$\tilde{W} = -\gamma\epsilon^2\sigma_\epsilon - 3a\frac{n}{N}A_1, \tag{3.29}$$

$$\tilde{D}\left(\frac{E}{N}\right)^2\frac{\epsilon}{\tilde{\sigma}_m} + \frac{\gamma k_B T_e}{e}\epsilon^2\sigma_\epsilon + 2a\frac{n}{N}\left(A_2 + \epsilon^{3/2}A_3\right), \tag{3.30}$$

$$\sigma_\epsilon = \sum_{k=elastic} \tilde{C}_0 + \tilde{R}, \tag{3.31}$$

$$\tilde{S} = \sum_{k=inelastic} \tilde{C}_0 + \tilde{R}. \tag{3.32}$$

For solving EEDF, we should impose the following boundary conditions at $\epsilon = 0$ and $\epsilon = \epsilon_{final}$ (maximum energy which is used), respectively.

$$\frac{\partial f}{\partial \epsilon} = 0, \tag{3.33}$$

$$f = 0. \tag{3.34}$$

Discretization of inelastic terms in the following fashion:

$$\int_{\epsilon_{i-1/2}}^{\epsilon_{i+1/2}} \tilde{S} d\epsilon = -P_i F_{0,i} + \sum_j Q_{i,j}. \tag{3.35}$$

The scattering-in and scattering-out terms are

$$Q_{i,j} = \sum_{inelastic} \gamma \int_{\epsilon_1}^{\epsilon_2} \epsilon \sigma_k exp[(\epsilon_j - \epsilon) g_j] d\epsilon, \tag{3.36}$$

$$P_i = \sum_{inelastic} \gamma \int_{\epsilon_{i-1/2}}^{\epsilon_{i+1/2}} \epsilon \sigma_k exp[(\epsilon_i - \epsilon) g_j] d\epsilon. \tag{3.37}$$

Diffusion, mobility and reaction rates can be calculated as follows:

$$\mu = -\frac{\gamma}{3N} \int_0^\infty \frac{\epsilon}{\tilde{\sigma}_m} \frac{\partial F_0}{\partial \epsilon} d\epsilon, \tag{3.38}$$

$$D = \frac{\gamma}{3N} \int_0^\infty \frac{\epsilon}{\tilde{\sigma}_m} F_0 d\epsilon, \tag{3.39}$$

$$k_k = \gamma \int_0^\infty \epsilon \sigma_k F_0 d\epsilon. \tag{3.40}$$

3.2 Two approaches: COMSOL Multiphysics and BOLSIG+ solvers

Comsol Multiphysics plasma module offer four options which are Boltzmann, Maxwell, Druyvesteyn, Generalized.

Boltzmann options offers as two-term approximation solver without defining equation which described EEDF. It can be solved as linear form EEDF or quadratic form EEDF.

The general form of Maxwell function that describes the EEDF is

$$f(\epsilon) = \xi^{-3/2} \alpha_1 exp(-\frac{\epsilon \alpha_2}{\xi}). \tag{3.41}$$

The general form of Druyvesteyn function that describes the EEDF is

$$f(\epsilon) = \xi^{-3/2} \alpha_1 exp((-\frac{\epsilon \alpha_2}{\xi})^2). \tag{3.42}$$

The general form of Generalized function that describe the EEDF is

$$f(\epsilon) = \xi^{-3/2} \alpha_1 exp((-\frac{\epsilon \alpha_2}{\xi})^g). \tag{3.43}$$

In the equations (3.47), (3.48), (3.49) g is a factor between 1 and 2. Detailed information can be found in the reference [41]. It can be noticed that when g=1 in the generalized form, it is Maxwell distribution function and when g=2 in the generalized form, it is Druyvesteyn distribution function[41]. Important note that Druyvesteyn distribution function gives more accurate results when ionization degree is lower. On the other hand, the Maxwellian distribution function gives more accurate results when ionization degree is relatively higher. In figure (3.1), it can be noticed that same cross section data can result in the different EEDF. In addititon to that this can lead to different reaction rates and transport coefficients. In figure (3.3) is the clear example that selected choice of distribution function can lead different results[42].

On the other hand, Bolsig+Solver provide us two option as distribution function which are Maxwellian and Non-Maxwellian. For this reason we validate our EEDF, transport coefficients and reaction rates selecting Maxwellian distribution function.

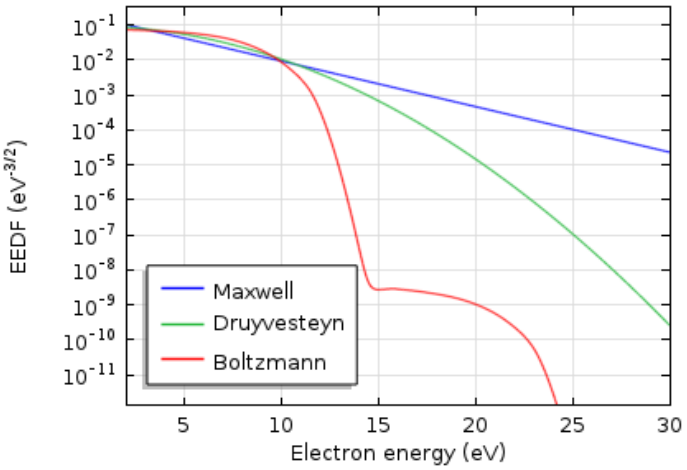

Figure 3.1: Comparison of EEDF vs electron energy. The mean electron energy is 5 eV, the electron density is $10^{16}(m^{-3})$, ionization degree is 10^{-9} [43]

.

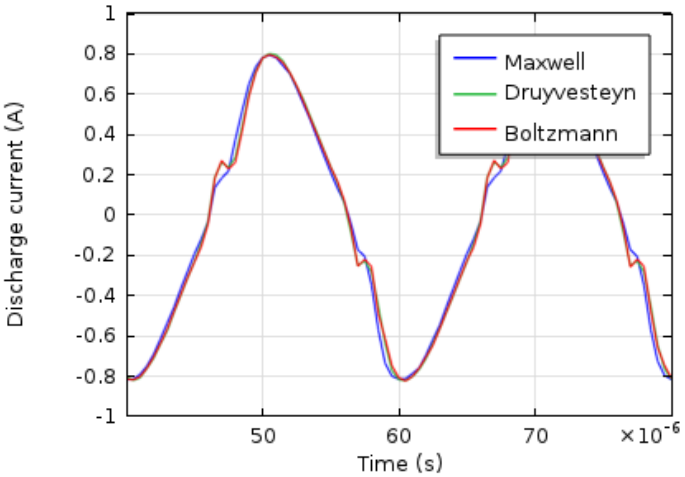

Figure 3.2: Total current in the grounded electrode with sinusoidal voltage with the frequency of 50kHz (DBD)[43]

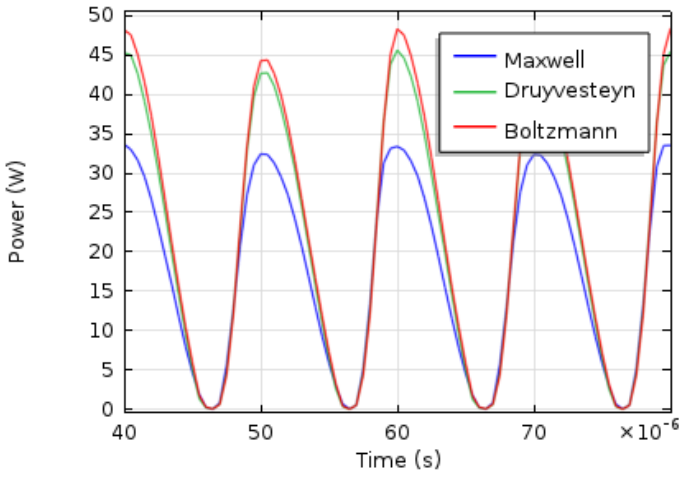

Figure 3.3: Instantaneously absorbed power in the plasma (DBD) [43]

.

3.3 Comparison of the kinetic (transport and rate) coefficients for electrons obtained from COMSOL Multiphysics and BOLSIG+ solvers, and also obtained with Maxwellian EEDF

Common EEDF provided by the Comsol Multiphysics plasma module and Bolsig+Solver is Maxwell. We check our reaction rates, transport coefficients. And reaction rates and transport coefficients are shared in the figures (3.4), (3.5), (3.6), (3.7).
Comsol Multiphysic plasma module uses temporal growth in calculations so that we use transport coefficients and reaction rates according to temporal growth in the extended fluid models.
In the figure (3.4), it can be said that diffusion and electron coefficients are inflated after mean energy pass 50 eV when temporal and spatial growth is not take in consideration in Maxwell EEDF. In the figures (3.5), (3.6), (3.7), similarly temporal and spatial growth calculations have deviated from the case which they did not count in Maxwell EEDF. Temporal and spatial growth calculations do not affect on the results in Nonmaxwellian EEDF.

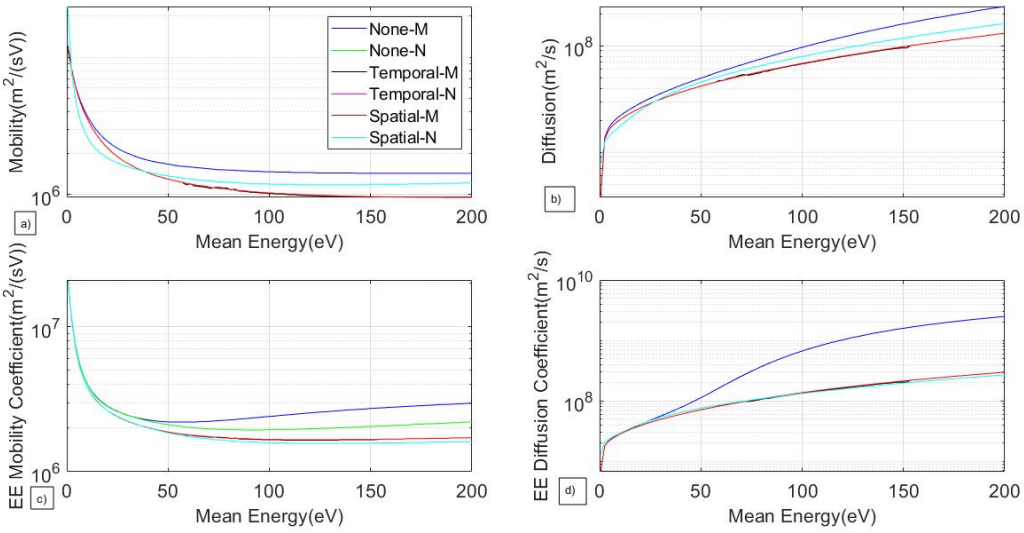

Figure 3.4: (a) Mobility (b)Diffusion (c) Electron energy mobility (d) Electron energy diffusion coefficients. M label indicates Maxwellian EEDF, N label indicates Nonmaxwellian EEDF.

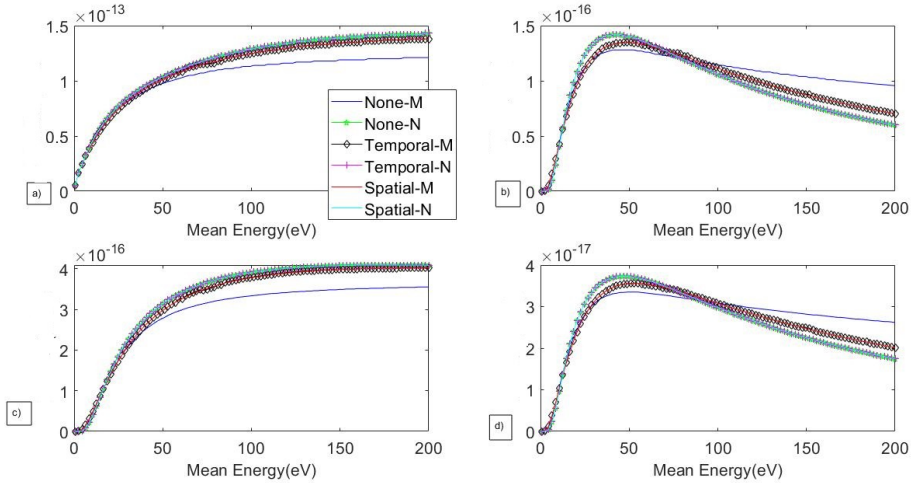

Figure 3.5: (a) R1 (b) R2 (c) R3 (d) R4 reactions in Table 1. M label indicates Maxwellian EEDF, N label indicates Nonmaxwellian EEDF.

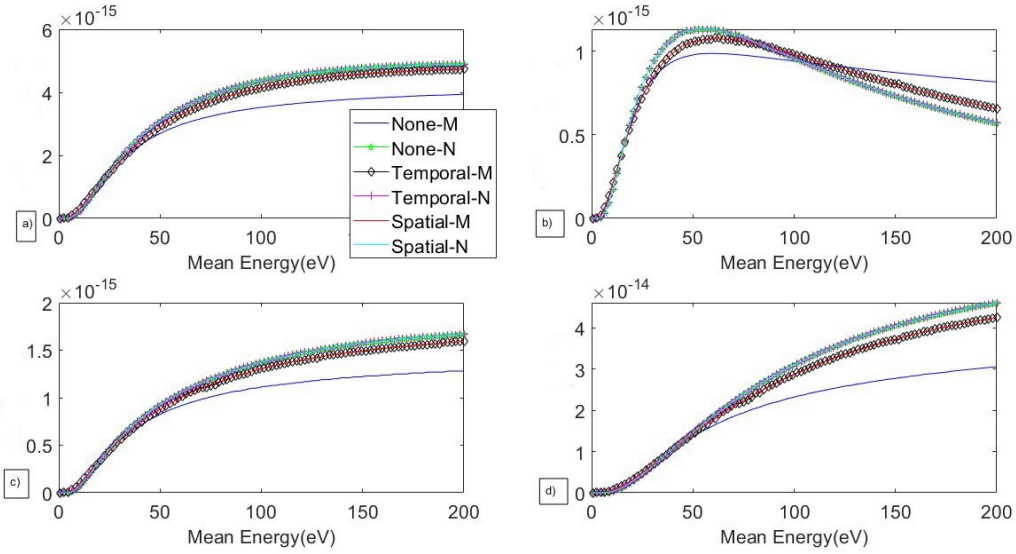

Figure 3.6: (a) R5 (b) R6 (c) R7 (d) R8 reactions in Table 1. M label indicates Maxwellian EEDF, N label indicates Nonmaxwellian EEDF.

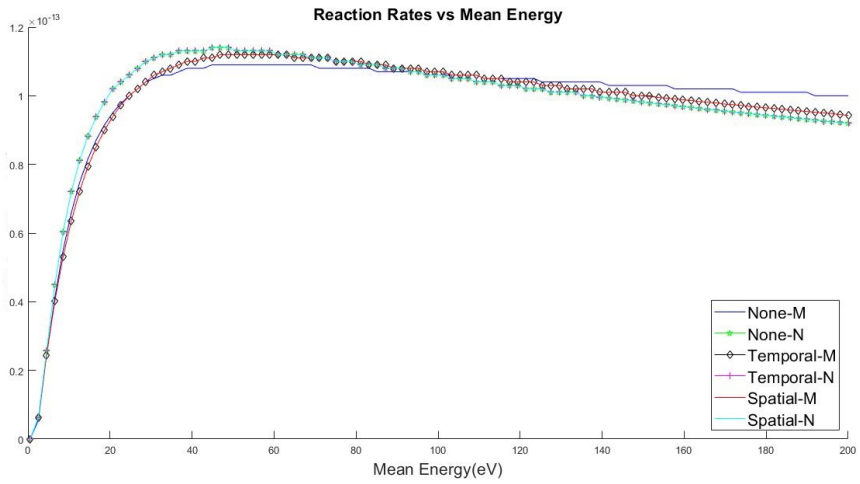

Figure 3.7: R9-R10-R11-R12 reactions in Table 1. Reaction rates are same for these four reactions. M label indicates Maxwellian EEDF, N label indicates Non-maxwellian EEDF.

CHAPTER 4

COMPARISON OF THE MODELS

Parameter regimes will be introduced and how the variables are used in the model will be explained. We investigate our fluid models as three sub-groups based on which fluid approach is used, which chemical reactions are used, and the form of EEDF. Effect of crucial parameters like pressure, driving frequency, voltage, dielectric coefficient (material type in dielectric) are investigated.

4.1 Basic characteristics of the DBD in Neon

The parameters used in extended models are introduced in Table 4.1 and Table 4.2. These two parameters regimes are also investigated with a simple fluid model approach. LFA approach is used in simple models so that the ionization is defined by the Townsend formula,

$$\alpha = \alpha_0 exp(-E_0/|E|) = Ape^{-Bp/|E|}, \tag{4.1}$$

A and B are taken from the [45] Mobility and diffusion coefficients are a function of E/p.

Contrary to simple models, LMEA approach is used in the extended models. In this approach, μ_e and D_e are the functions of electron temperature T_e.

$$T_e = w/n_e, \tag{4.2}$$

where w is the electron energy density, n_e is the electron density. The gas density is scaled to scalar pressure with using $N_g = pN_0$ relationship.

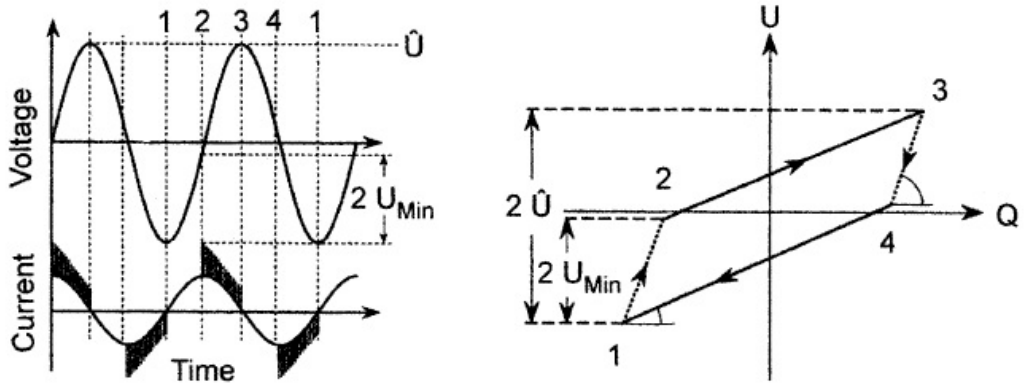

Figure 4.1: Microdischarge activity and corresponding voltage-charge graph from [49]

The breakdown voltage to start gas discharge between electrodes is formulated as a function of gap length and pressure is formulated by Paschen's Law. For example, the fact that 3.7 MV is the breakdown voltage to produce 1 meter arc in the air at 273.15K and $10^5 Pa$; on the other hand, 327 V is the breakdown voltage to produce 7.5 μm arc in the air at 273.15K and $10^5 Pa$. An interesting fact that the 7.5 μm arc discharge needs 11.78 times more the electric field strength than 1 meter long arc. Investigating the effect of gas pressure in Ne is very crucial to the formation of current peak, because the need of electric field strength is depend on pressure and gap length. Width of current formation in DBD can be manipulated by pressure and gap length. In the section (4.1.2), we changed pressure 1 torr to 100 torr in parameter set-1 to observe the results.

Optimal the driving frequency range for the DBD system is 1 kHz to 10Mhz. Microdischarges occurs two times in the one period, it can be seen this time domains (the path from point 2 to point 3, the path from point 4 to point 1) in the figure (4.1). The circuit equivalent approach is described in the work from [46] for the DBD system is described in the figure (2.1). According to this approach slope of the path from point 2 to point 3 or the path from point 4 to point 1 gives C_{cell} described as

$$\frac{1}{C_{cell}} = \frac{1}{C_d} + \frac{1}{C_g}, \tag{4.3}$$

where C_d is the capacitance of dielectric, C_g is the capacitance of the gas gap. The

slope of the path from point 3 to point 4 or the path from point 1 to point 2 gives C_d. For the same peak voltage, the power in the system is proportional to the driving frequency[46]. The equivalent circuit approach is described above basically, the more complicated understanding is required for experimental studies. For numerical studies, total, conducting and displacement current are calculated. All in all, currents vs voltage graphs are useful to get information about ignition and decay of discharge [46].

There is a required breakdown voltage to ignite the plasma. Study shows that increasing voltage from certain point result in microdischarges in the current formation. And also, it is crucial to note that this effect is responsible by plasma current, is not from development of displacement current [50].

Table 4.1: Parameters Set-1

Symbol	Value	Unit	Definition
L	0.002	m	Discharge gap
L_e	0.002	m	Dielectric barrier length
p	100	Torr	Pressure
μ_e	$\mu_e(T_e)$	$m^2/(Vs)$	Electron mobility
μ_i	$\mu_i(E/p)$	$m^2/(Vs)$	Ion mobility
D_e	$\mu_e(T_e)$	m^2/s	Electron diffusion coefficient
D_i	$\mu_i T_i$	m^2/s	Ion diffusion coefficient
N_0	3.29×10^{24}	$1/(m^3 Torr)$	Gas density of 100 Torr
$T_g = T_i$	0.02499	eV	Ion or gas temperature
T_e	w/n_e	eV	Electron temperature
γ	0.1	-	Secondary emission coefficient

4.1.1 Current-Voltage characteristics of the models

Current-voltage characteristics in the figure (4.2) based on the extended fluid approach and it include the first eight chemical reactions from table-1 at chapter two.

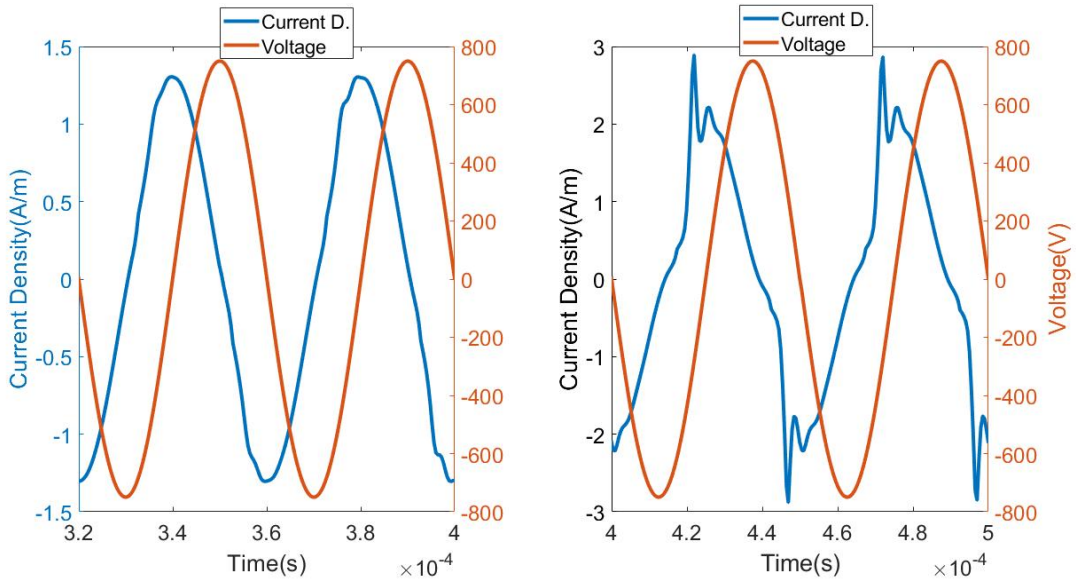

Figure 4.2: Current vs voltage graphs. The left graph is in the Parameter Set-1 from Table 4.1, 25 kHz (750V) the driving frequency, relative permittivity 5. The right graph is in the Parameter Set-2 from Table 4.2, 20 kHz (750V) the driving frequency, relative permittivity 5.

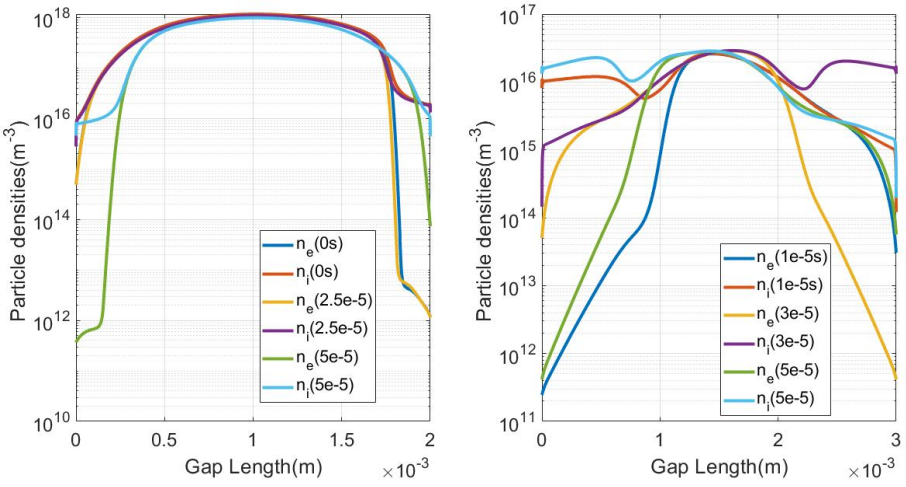

Figure 4.3: Particle densities vs Gap length graphs. The left graph is in the Parameter Set-1 from Table4.1, 25 kHz (750V) the driving frequency, relative permittivity 5. The right graph is in the Parameter Set-2 from Table 4.2, 20 kHz (750V) the driving frequency, relative permittivity 5.

Table 4.2: Parameters Set-2

Symbol	Value	Unit	Definition
L	0.003	m	Discharge Gap
L_e	0.001	m	Dielectric Barrier Length
p	100	Torr	Pressure
μ_e	$\mu(T_e)$	$m^2/(Vs)$	Electron mobility
μ_i	$\mu(E/p)$	$m^2/(Vs)$	Ion mobility
D_e	$D_e(T_e)$	m^2/s	Electron diffusion coefficient
D_i	$\mu_i T_i$	m^2/s	Ion diffusion coefficient
N_0	3.29 $\times 10^{24}$	$1/(m^3 Torr)$	gas density of 100 Torr
$T_g = T_i$	0.02499	eV	ion or gas temperature
T_e	$T_e = w/n_e$	eV	electron temperature
γ	0.03	-	Secondary emission coefficient

And also Maxwellian electron energy distribution function is used for calculation of reaction rates and transport coefficients at this parameter sets. It can be said that current lagging against voltage at both graphs in the figure (4.2). It is very reasonable that dielectrics introduce the plasma system to capacitive behaviour. Even if, there are slight shifts around some time regions. And also, there are different shape of currents between both figures. There is nearly perfect sinusoidal shape current in model at the left graph. On the other hand, it seems that sinusoidal shape current superpositions with microdischarges in the model at the right graph.

4.1.2 Electron-Ion and Excited Particles Density Profiles

In the left graph in the figure (4.3) quasi-neutrality is achieved except the regions are closer to dielectric walls. Similar findings can be said about parameters set-2 model in the right graph in the figure (4.3) but it is not smooth as the previous model. Excited particles densities vary from each other distinctively, because chemical reactions are different than each other. When we compare two graphs, parameter set-2' particle distributions at the right graph in the figure (4.4) has nearly 10 times bigger than

parameter set-1' particle distributions at the left graph in the figure (4.4). Longer charge gap and different the driving frequency may lead to this result.

4.1.3 Electric Field and Potential Profiles

The left graph in the figure (4.5) and (4.6), -2 mm to 0 mm and 2 mm to 4 mm are dielectric barriers and area between these to the region (0 mm to 2 mm) is the gap length. The right graph in the figure (4.5), -1 mm to 0 mm and 3 mm to 4 mm are dielectric barriers and area between these to region (0 mm to 1 mm) is the gap length. In the graphs at the figure (4.5), electric fields lines are straight and the lines are changed in time points to time point. This generates displacement current in the dielectric barriers. And also electric fields are changing significantly closer points to the dielectric wall at the gap length.
The graphs in the figure (4.6), potential lines are changing significantly at the quarter of the period (50μs for the left graph and 62.5 μs for the right graph) and the third quarter of the period (70μs for the left graph and 87.5 μs for the right graph) at dielectric barriers. Potential lines are linear at any time point because the electric field in the dielectrics does not change in position for any time point. Gap voltage in the plasma (the gap length) are nonlinear but their magnitudes are small compare to dielectric barriers.

4.1.4 Current Density Profiles

Both graphs in the figure (4.7), every $J_D(Left)$ and $J_D(Right)$ are the displacement current densities at the dielectrics and they are straight lines. In figure (4.6) electric fields do not change in the position but they change with time so that the displacement current density behaviour at the dielectrics is expected. Sum of J_e (Electron current density) and J_i (Ion current density) is equal to J (the conductor current density in the plasma). J_D is the displacement current density in the plasma. J_s is the sum of the the displacement current density in the plasma and the conductor current density in the plasma. Both graphs in the figure (4.7), $J_D(Left)$, $J_D(Right)$ and J_s are same through the DBD systems because of the conservation the charge.

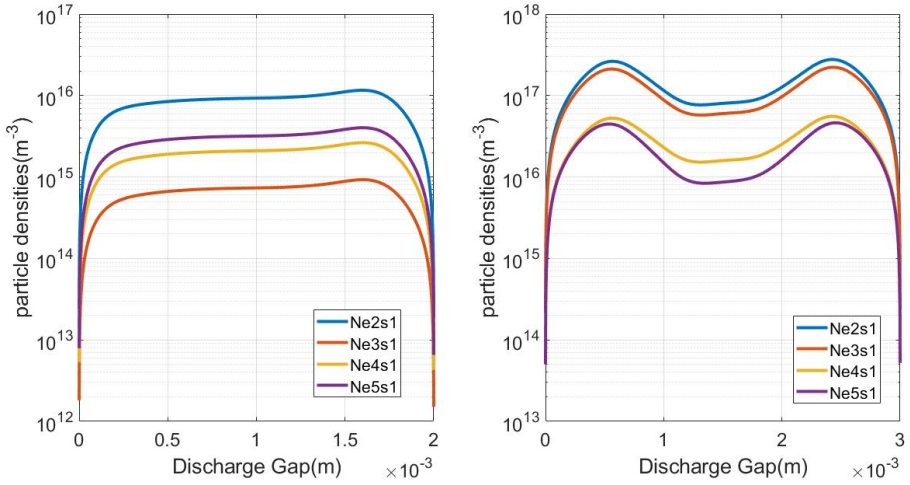

Figure 4.4: Metastable and resonant species at the first time period. The left graph is in the Parameter Set-1 from Table4.1, 25 kHz (750V) the driving frequency, relative permittivity 5 , period 40μs. The right graph is in the Parameter Set-2 from Table 4.2, 20 kHz (750V) the driving frequency, relative permittivity 5, period 50μs

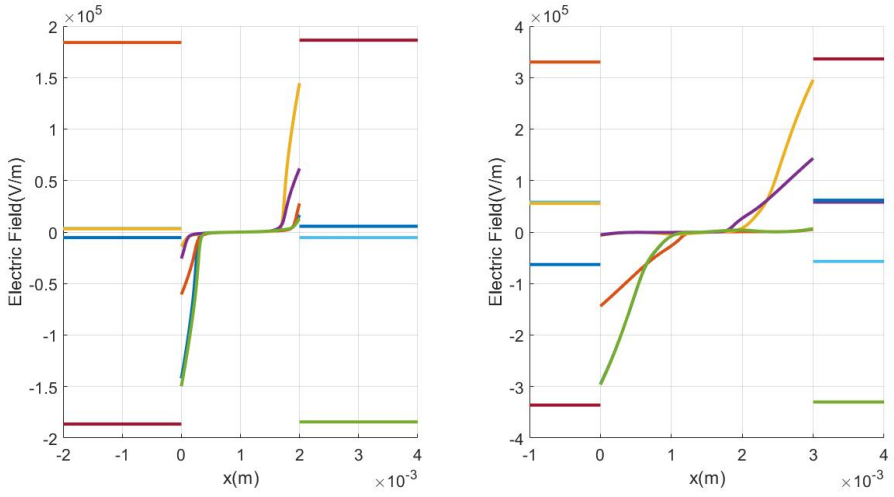

Figure 4.5: Electric fields vs position. The left graph is in the Parameter Set-1 from Table4.1, 25 kHz (750V) the driving frequency, relative permittivity 5 , period 40μs and field lines from 40μs, 50μs, 60μs, 70μs, 80μs time points. The right graph is in the Parameter Set-2 from Table 4.2, 20 kHz (750V) the driving frequency, relative permittivity 5, period 50μs and field lines from 50μs, 62.5μs, 75μs, 87.5μs, 100μs time points.

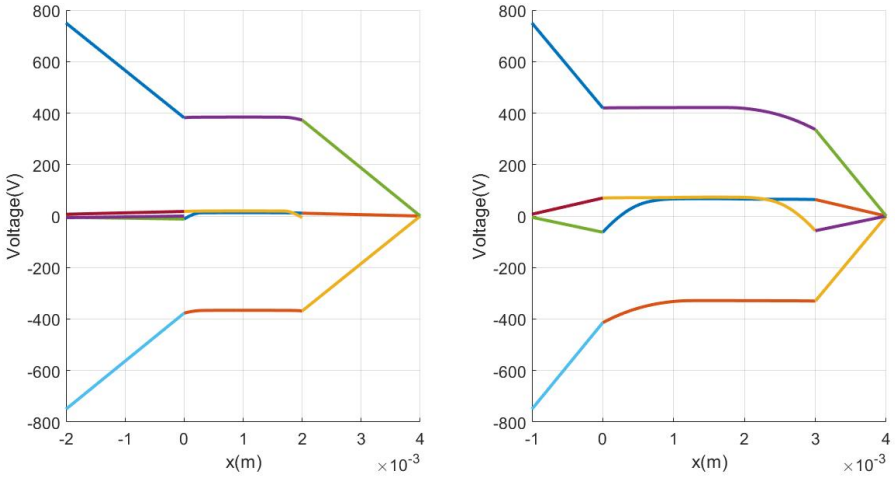

Figure 4.6: Potential Lines vs position. The left graph is in the Parameter Set-1 from Table4.1, 25 kHz (750V) the driving frequency, relative permittivity 5 , period $40\mu s$ and field lines from $40\mu s$, $50\mu s$, $60\mu s$, $70\mu s$ time points. The right graph is in the Parameter Set-2 from Table 4.2, 20 kHz (750V) the driving frequency, relative permittivity 5, period $50\mu s$ and field lines from $50\mu s$, $62.5\mu s$, $75\mu s$, $87.5\mu s$ time points.

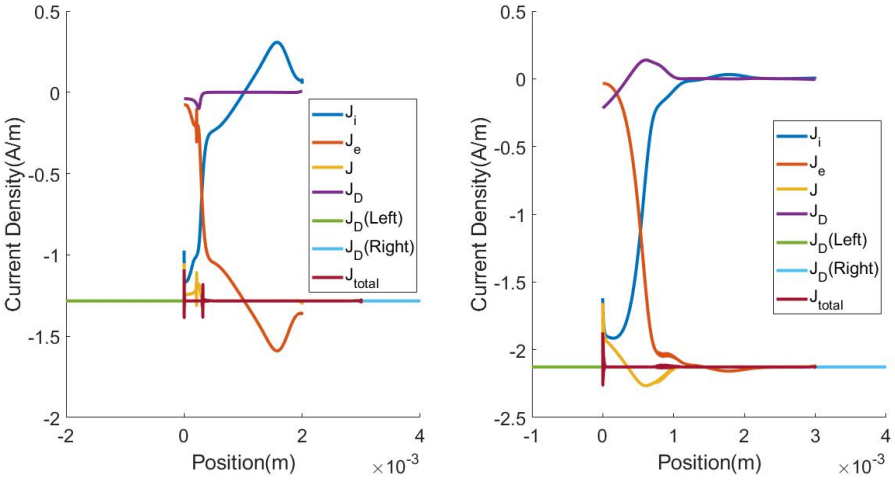

Figure 4.7: Current densities vs position. The left graph is in the Parameter Set-1 from Table4.1, 25 kHz (750V) the driving frequency, relative permittivity 5 , at $40\mu s$. The right graph is at $50\mu s$ time point in the Parameter Set-2 from Table 4.2, 20 kHz (750V) the driving frequency, relative permittivity 5, at $50\mu s$.

4.2 Effect of different plasma-chemical approaches (within the extended fluid model) on the DBD characteristics

We analyze our parameter set-1 and parameter set-2 in two EEDF approaches. First one is Maxwell EEDF and the second one is Nonmaxwell EEDF, which are two options in the Bolsig+Solver. Also, first, eight chemical reactions are investigated as the first version of the study. All twelve reactions are investigated as the second version of this study. Version 1 abbreviated as v1 and version 2 investigated as v2 in the figures. M and N are used as abbreviations for Maxwell EEDF and Nonmaxwelian EEDF respectively.

A closer look at both graphs in the figure (4.8), it seems that there is no significant effect of current when taking account on different chemical reactions (v1-v2) for our models (0.1 percent to and 0.5 percent is scale of difference in any time data points). On the other hand, different EEDF approaches lead to minor changes in current profiles, even if the shape and peak of the current are nearly same (0.1 percent to 2.0 percent is the scale of difference in any time data points).

In the graphs in the figures (4.9), (4.10) , reactions are from table 1 in chapter two. These reactions are accounted source term form S_e and S_i in the extended model. The eighth reaction source term is greater but it is not continuous after 0.25 mm point in the left graph of the figure (4.9). On the other hand, in the right graph in the figure (4.9), eighth reaction source term does not exist after around 0.4 mm . From ninth reaction to twelfth reaction source term are close to each other but turning points are different. We can conclude that eighth reaction is the dominant reaction for source term and the other reactions have a minor effect on source term. And also the choice of EEDF has a major effect on source term numerically.

In the left graph in the figure (4.10), Maxwellian eighth reaction source term is not continuous in the gap length. In the right graph in the figure (4.10), eighth reaction source terms are different from each other with respect to their turn around point. Their shape is continuous. Still, the choice of EEDF has a major effect and eighth reaction is dominant as source term compare to other reactions.

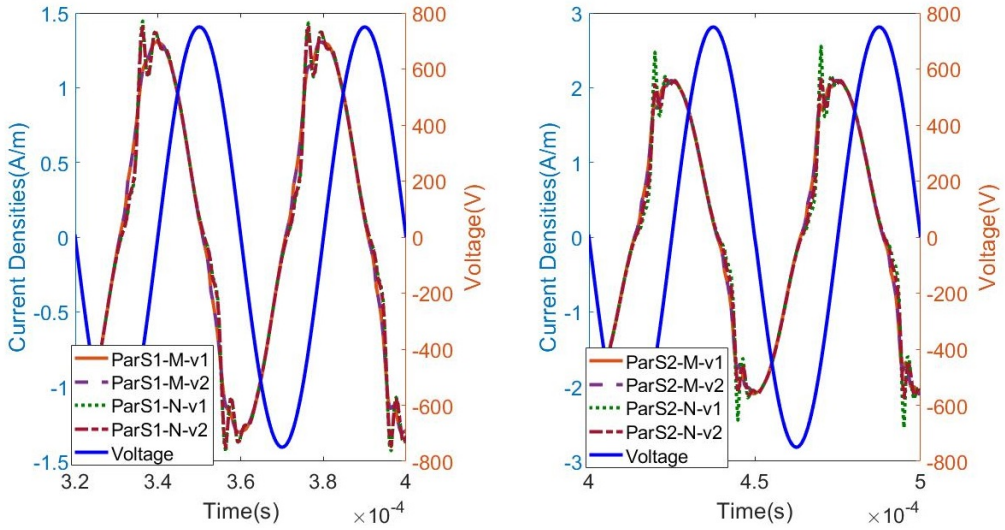

Figure 4.8: Comparisons current voltage profiles according to chemical reaction and EEDF. ParS1, ParS2 is an abbrivation from Table 4.1 and Table 4.2 respectively.

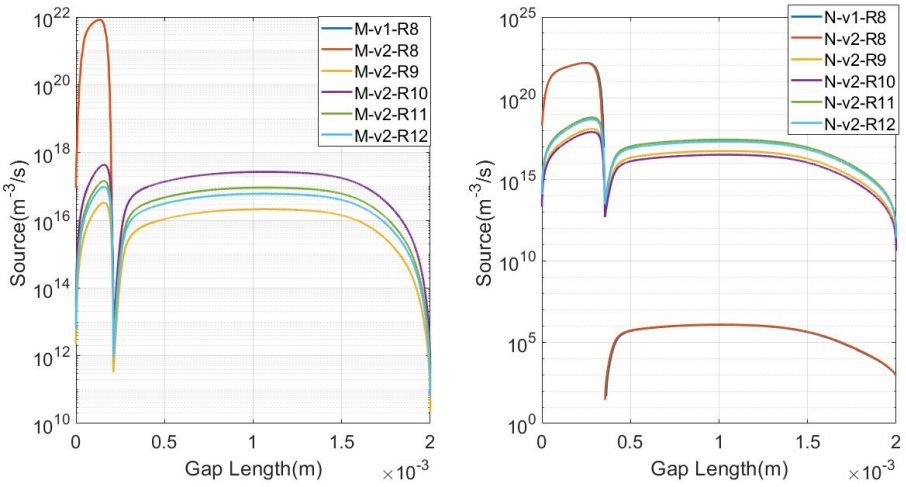

Figure 4.9: Source profiles at the first time period for ParS1

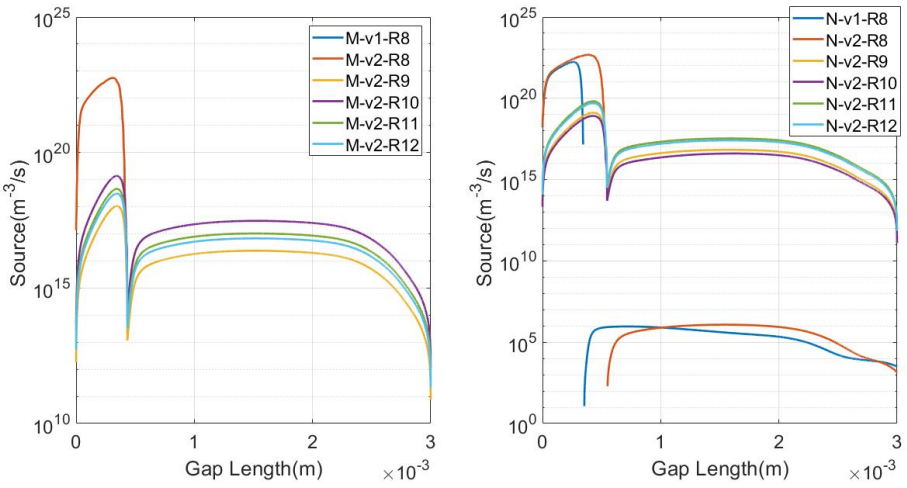

Figure 4.10: Source profiles at the first time period for ParS2

4.2.1 Difference in the DBD characteristics obtained from extended and simple fluid models

Electron densities are 10^6 times greater, ion densities are 10^6 is smaller at point 0 m in the gap length; on the other hand, electron densities and ion densities are close each other at 2 mm point when comparing simple model to extended model at the left graph (parameter set-1) in figure (4.11). Extended model predicts particle densities 100 times greater than the simple model for parameter set-1 in the figure (4.11). The same comparison for parameter set-2 in the figure (4.11), electron ion densities are nearly same at point 0 m and the simple model approach over calculate particle densities at point 2 mm point compare to the extended model approach.

Compare to figure (4.12) and (4.8) only difference is that the simple model current density as the light blue colour line is added to figure (4.12). The simple model current developments are close numerically to other current densities for the same parameter regime but the shape is perfectly sinusoidal in the graphs in the figure (4.12).

4.2.2 Effect of the Ne gas pressure on the DBD characteristics

When gas pressure change 100 torr to 10 torr current density profile shifts from the left to the right even though the magnitude of them are close to each other. When

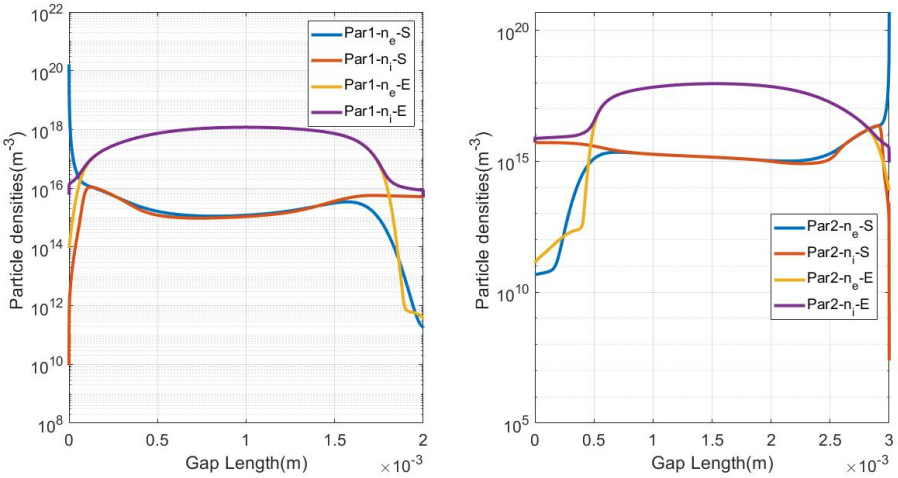

Figure 4.11: Particle densities vs position where voltage value 750 V in driving source is 750 V. ParS1, ParS2 is an abbreviation from Table 4.1 and Table 4.2 respectively.S, E stand for simple model, extended model approach respectively. .

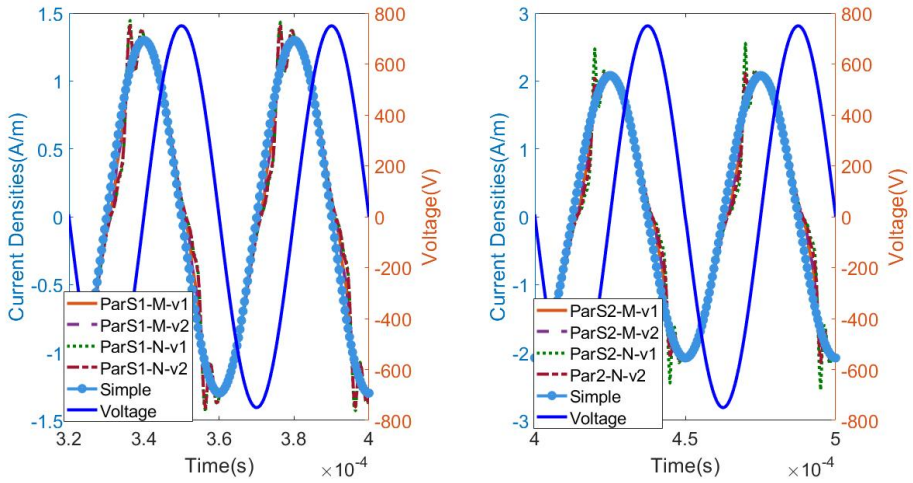

Figure 4.12: Current densities vs position. ParS1, ParS2 is an abbreviation from Table 4.1 and Table 4.2 respectively.

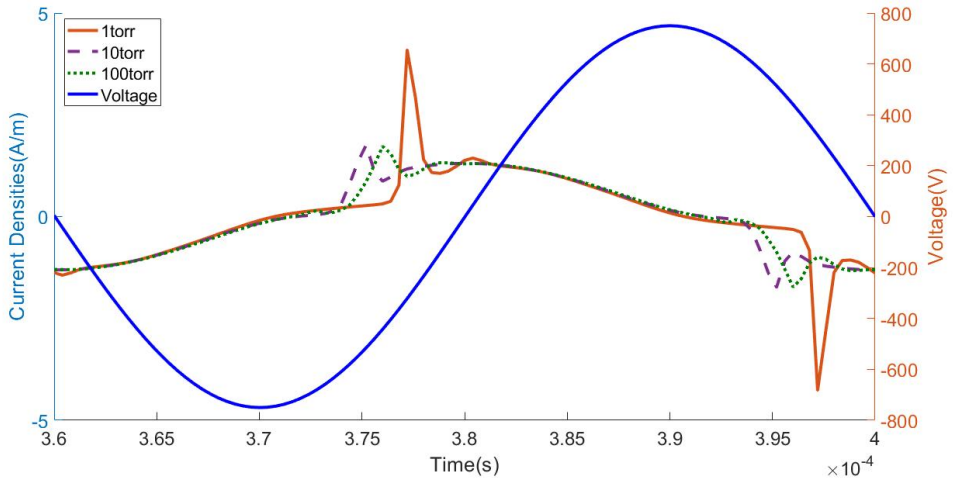

Figure 4.13: Comparison of current densities for different pressure values . Models from extended fluid approach, parameter set-1, first eight reactions are included in the table 1 from chapter two

we compare 1 torr' current density profile to other 10 and 100 torr' current density profile, 1 torr' current density profile shifts to right to them and nearly 4 times greater than their peak value.

The pressure is crucial control parameter for current density profile as expected due to Paschen' Law. Width of current density may be manipulated by changing pressure and gap length. For two and three dimensional models, pressure and gap length of plasma should be manipulated for pattern formation in the current density profiles for two and three dimensional models.

4.2.3 Effect of the driving sinusoidal voltage on the DBD characteristics

Increasing voltage value 1000V to 2000 V is resulted in increasing the total current density peak in the figure (4.14). This is an expected result due to Ohm's law. Current profiles in the figure (4.14), microdischarges may interfere with each other. Lowering voltage to observe smaller or bigger width of the current density may not be achieved. Changing voltage value may have no effect on pattern formation.

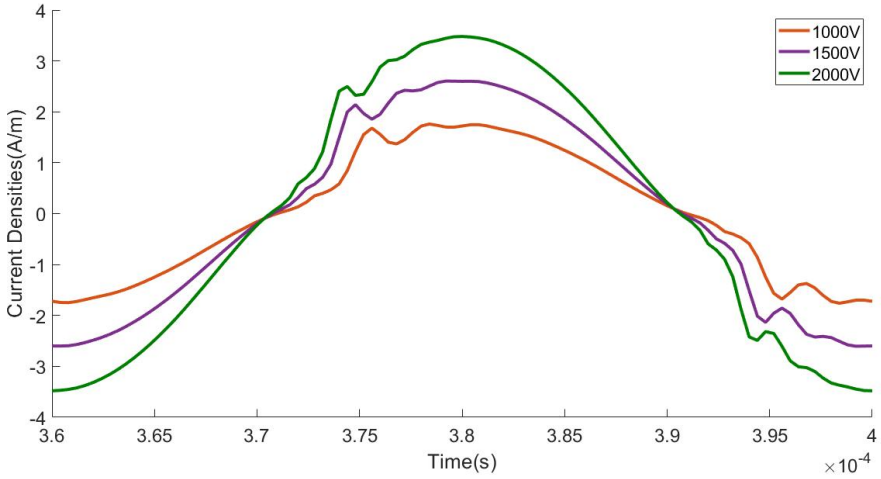

Figure 4.14: Comparison of current densities for different voltage values . Models from extended fluid approach, parameter set-1, first eight reactions are included in the table 1 from chapter two

4.2.4 Effect of the dielectric constant on the DBD characteristics

As a circuit element capacitive reactance is,

$$X_C = \frac{1}{2\pi f C} \tag{4.4}$$

where f is the driving frequency and C is the capacitance. Capacitance inversely proportional to a dielectric constant so that when dielectric constant is increased, capacitive reactance is decreased. If we think the DBD system as the circuit impedance of the system will be lower and current density will be higher. Even if this is very simple approximation, figure (4.15) shows that when the dielectric constant is increased, the current density will be higher. When dielectric constant 2 in the figure (4.15), the current density is different than the other dielectric constant profiles when his peak is reversed at the end of the graph. Lower dielectric constants may give more interesting results for self organization patterns in the DBD and should be investigated for their current density profile behaviours.

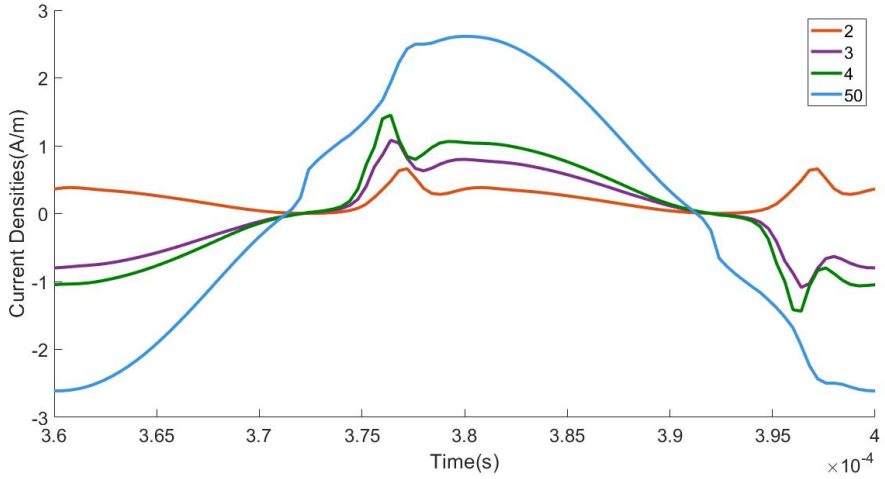

Figure 4.15: Comparison of different dielectric constants on current densities for parameter set-1, Maxwellian EEDF, first eight reactions are included

4.2.5 Effect of the driving frequency on the DBD characteristics

In the equation(4.4), the driving frequency is one of the parameter decide capacitive reactance. When the driving frequency is increased, capacitive reactance is decreased and the impedance of the DBD system is decreased. This leads to increased current density in the plasma. The figure (4.16) shows that this approximation is a valid but better understanding of current density needs much broad explanation. It can be said that the driving frequency is proportional to current densities in DBD system.

The instantaneous dissipated power for the plasma,

$$P(t) = U_g(t)I(t), \tag{4.5}$$

where U_g is the potential difference between the dielectric walls and I(t) is the discharge current, the total current density for our system. The instantaneous dissipated power are calculated from the equation (4.6) and it is confirmed that for same peak voltage (750 V), the driving frequency is proportional to the power in the system [46].

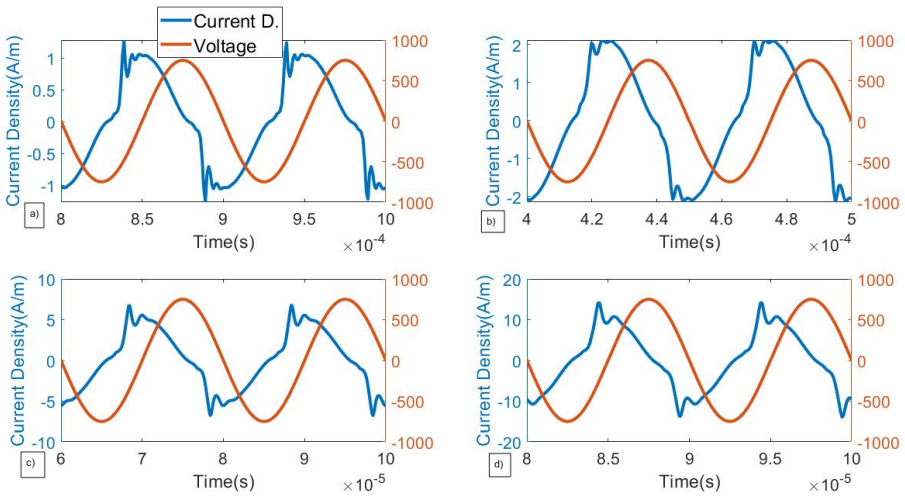

Figure 4.16: Comparison of driving frequency on current densities for parameter set-1, Maxwellian EEDF, first eight reactions are included. (a) 10 kHz (b) 20 kHz (c) 50 kHz (d) 100 kHz

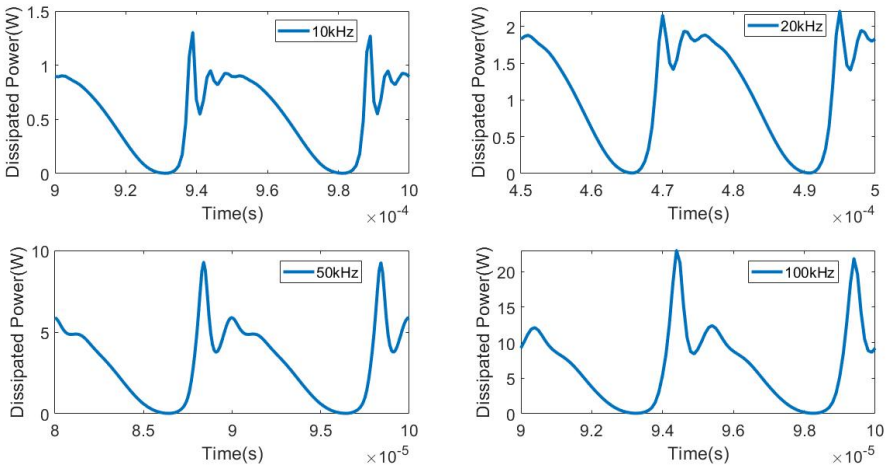

Figure 4.17: Comparison of driving frequency on dissipated power for the plasma for parameter set-1, Maxwellian EEDF, first eight reactions are included.

CHAPTER 5

DISCUSSION

One dimensional DBD models are developed for Neon gase with using Comsol Multiphysics. In the simple models, transport and rate coefficients are the function of a local electric field. In the extended model, the coefficients are a function of the local mean energy. Different fluid approaches result in divergent findings in terms of current density and particle density profiles. Choice of EEDF affects the results in a minor way; in other words, it does not provide interesting results. Reaction eighth from table 1 in chapter two contributes dominant source term, reactions from ninth to twelfth has a very small contribution to source term so that versions of the models do not provide a significant difference between them. Lowering the pressure results in shrinking the width of current density line. Changing voltage value has no significant effect on the shape of the current density other than the magnitude of it for our parameter regimes but it will increase the activity of microdischarges . Adjusting pressure and gap length has a nonlinear relationship that these two parameters may have a great impact on pattern formation in the DBD systems. Effect of the driving voltage value is examined. Changing the dielectric constant give expected result but lowering the the dielectric constant may result in a significant change on the current density profile. While the same voltage value, increasing frequency results in proportionally increased current density and dissipated power from the plasma.

REFERENCES

[1] Post M, Cork T. *Overview of plasma flow control: concepts, optimization, and application*. AIAA Paper 2005-0563; 2005.

[2] Kunhardt E. *Generation of large volume atmospheric pressure nonequilibrium plasmas.* IEEE Trans Plasma Sci 2000;28(1):189–99.

[3] J.P.Lebrun *Plasma-assisted processes for surface hardening of stainless steel* Thermochemical Surface Engineering of Steels.;2015, Pages 615-632

[4] B.Marcandalli, C.Riccardi *Plasma treatments of fibres and textiles* Plasma Technologies for Textiles. 2007, Pages 282-300

[5] E.Angelini ,S.Grassini *Corrosion and Conservation of Cultural Heritage Metallic Artefacts* European Federation of Corrosion (EFC) Series 2013, Pages 552-569

[6] K.Vaideki *Plasma technology for antimicrobial textiles* Antimicrobial Textiles Woodhead Publishing Series in Textiles 2016, Pages 73-86

[7] P.Blanchet, V.Landry *Nanocomposite coatings and plasma treatments for wood-based products* Wood Composites 2015, Pages 335-355

[8] Akira Mizuno, Robert D. Short, *Chapter 3 - Plasma Biological Science in Various Species* Plasma Medical Science 2019, Pages 109-171

[9] Akira Mizuno, Robert D. Short, *Non-thermal food pasteurization processes: an introduction* Case Studies in Novel Food Processing Technologies, 2010, Pages 1-18

[10] S.Foong-Cunningham, E.L.C.VerkaarK, .Swanson *Microbial decontamination of fresh produce* Microbial Decontamination in the Food Industry, 2012, Pages 3-29

[11] lH.Würz,B.Bazylev, F.Kappler, I.Landman, S.Pestchanyi, G.Piazza *Fusion*

Technology 1996 Proceedings of the 19th Symposium on Fusion Technology, Lisbon, Portugal, 16–20 September 1996 1997, Pages 191-196

[12] GarryMcCracken, PeterStott *Fusion (Second Edition)* 2013, Pages 91-105

[13] PierreJaeglé *Vacuum Ultraviolet Spectroscopy* Experimental Methods in Physical Sciences Volume I, 2000, Pages 101-118

[14] Dustin H.Froula, Siegfried H.Glenzer, Neville C.Luhmann, Jr.JohnSheffield *Chapter 2 - Scattered Power Spectrum* Plasma Scattering of Electromagnetic Radiation (Second Edition) 2011, Pages 31-44

[15] L.A.Fisk, G.Gloeckler *Chapter 15 - Common Spectrum of Particles Accelerated in the Heliosphere: Observations and a Mechanism* Kappa Distributions Theory and Applications in Plasmas 2017, Pages 569-608

[16] Holly Zell *The Heliosphere.*
$https://www.nasa.gov/mission_pages/sunearth/science/Heliosphere.html, Jan.22, 2013$

[17] R.H.HenneK., A.Friedrich *APPLICATIONS – TRANSPORTATION | Auxiliary Power Units: Fuel Cells* Encyclopedia of Electrochemical Power Sources 2009, Pages 157-173

[18] Margaret Galland, KivelsonFranBagenal *Chapter 7 - Planetary Magnetospheres* Encyclopedia of the Solar System (Third Edition) 2014, Pages 137-157

[19] P.Falkner, R.Schulz *10.23 - Instrumentation for Planetary Exploration Missions* Treatise on Geophysics (Second Edition) Volume 10, 2015, Pages 719-755

[20] Graeme G.Lister, John F.Waymouth *Light Sources* Encyclopedia of Physical Science and Technology (Third Edition) 2003, Pages 557-595

[21] M.Sato, S.W.Kim, Y.Shimomura, T.Hasegawa, K.Toda, G.Adachi *Chapter 278 - Rare Earth-Doped Phosphors for White Light-Emitting Diodes* Elsevier Handbook on the Physics and Chemistry of Rare Earths Volume 49, 2016, Pages 1-128

[22] K.Dialynas, C.P.Paranicas, J.F.Carbary, M.Kane, S.M.Krimigis, B.H.Mauk *Chapter 12 - The Kappa-Shaped Particle Spectra in Planetary Magnetospheres* Kappa Distributions Theory and Applications in Plasmas 2017, Pages 481-522

[23] M.C.Ramkumar, P.Cools, A.Arunkumar, N.De Geyter, R.Morent, V.Kumar, S.Udaykumar, P.Gopinath, S.K.Jaganathan, K.N.Pandiyaraj *Polymer coatings for biocompatibility and reduced nonspecific adsorption* Functionalised Cardiovascular Stents 2018, Pages 155-198

[24] LadislavCvrček, MartaHoráková *Chapter 14 - Plasma Modified Polymeric Materials for Implant Applications* Non-Thermal Plasma Technology for Polymeric Materials Applications in Composites, Nanostructured Materials and Biomedical Fields 2019, Pages 367-407

[25] Kenth S.Johansson *Surface Modification of Plastics* Applied Plastics Engineering Handbook (Second Edition) Processing, Materials, and Applications Plastics Design Library 2017, Pages 443-487

[26] T.Herbert *Atmospheric-pressure cold plasma processing technology* Plasma Technologies for Textiles Woodhead Publishing Series in Textiles 2007, Pages 79-128

[27] Sina Ebnesajjad *Surface Treatment of Fluoropolymers for Adhesion* Fluoroplastics (Second Edition) Volume 2: Melt Processible Fluoropolymers - the Definitive User's Guide and Data Book 2015, Pages 564-588

[28] AkioHirose, KeizohHonda, Kojiro F.Kobayashi *Nitride Reinforced Tial Formed be Reactive Low Pressure Plasma Spraying* Novel Materials Processing by Advanced Electromagnetic Energy Sources Proceedings of the International Symposium on Novel Materials Processing by Advanced Electromagnetic Energy Sources March 19–22, 2004, Osaka, Japan 2005, Pages 411-414

[29] Shrikaant Kulkarni *Chapter 3 - Plasma Assisted Polymer Synthesis and Processing* Non-Thermal Plasma Technology for Polymeric Materials Applications in Composites, Nanostructured Materials and Biomedical Fields 2019, Pages 67-93

[30] Jose Luis Ballester, Igor Alexeev, Manuel Collados, Turlough Downes, Robert F. Pfaff, Holly Gilbert, Maxim Khodachenko, Elena Khomenko, Ildar F. Shaikhislamov, Roberto Soler, Enrique Vazquez-Semadeni,

Teimuraz Zaqarashvili *Partially Ionized Plasmas in Astrophysics* https://arxiv.org/abs/1707.07975

[31] Eckhard Wörner,Christoph Wild *Polycrystalline CVD Diamond for Industrial Applications* Reference Module in Materials Science and Materials Engineering Comprehensive Hard Materials Volume 3, 2014, Pages 365-377

[32] J.L.Shohet *Plasma Science and Engineering* Encyclopedia of Physical Science and Technology (Third Edition) 2003, Pages 401-423

[33] A. M. Turing *The Chemical Basis Of Morphogenesis* Philosophical Transactions of the Royal Society of London. Series B, Biological Sciences, Vol. 237, No. 641. (Aug. 14, 1952), pp. 37-72

[34] Bernecker B *Formation de structures et phenom´ enes‘ d'auto-organization dansles Decharges´ a Barri‘ ere‘ Dielectrique* 2010 PhD Dissertation University of Toulouse

[35] T Callegari, B Bernecker and J P Boeuf *Pattern formation and dynamics of plasma filaments in dielectric barrier discharges* Plasma Sources Sci. Technol. 23 (2014)

[36] Bernecker B, Callegari T, Blanco S, Fournier R and Boeuf J P *Hexagonal and honeycomb structures in Dielectric Barrier Discharges* 2009 Eur. Phys. J. Appl. Phys. 47 22808

[37] Umran Inan, Marek Gołkowski *Principles of Plasma Physics for Engineers and Scientists* Cambridge University Press, Page 84-85

[38] Umran Inan, Marek Gołkowski *Principles of Plasma Physics for Engineers and Scientists* Cambridge University Press, Page 100

[39] Umran Inan, Marek Gołkowski *Principles of Plasma Physics for Engineers and Scientists* Cambridge University Press, Page 261-262

[40] Umran Inan, Marek Gołkowski *Principles of Plasma Physics for Engineers and Scientists* Cambridge University Press, Page 90-94

[41] H.B. Milloy and R.O. Watts *On the Validity of the Two-term Approximation in the Solution of Boltzmann's Equation for Electron Motion* Aust. J. Phys., vol 30, pp 73, 1977.

[42] G. K. Grubert, M. M. Becker, and D. Loffhagen *Why the local-meanenergy approximation should be used in hydrodynamic plasma descriptions instead of the local-field approximations* Physical Review E, 80:036405, 2009.

[43] Annette Pahl *COMSOL Blog: Electron Energy Distribution Functions* https://www.comsol.com/blogs/electron-energy-distribution-function/ August 4, 2014

[44] *TRINITI database, www.lxcat.net, retrieved on August 21, 2020.*

[45] *Yuri P. Raizer. Gas Discharge Physics. Springer, 2001.*

[46] Andrei V. Pipa , Ronny Brandenburg *The Equivalent Circuit Approach for the Electrical Diagnostics of Dielectric Barrier Discharges: The Classical Theory and Recent Developments*

[47] Duddell, W. *On the resistance and electromotive forces of the electric arc", Philosophical Transactions of the Royal Society A: Mathematical, Physical and Engineering Sciences, 203 (359–371): 512–15*

[48] Almarshoud, A. F. *Performance of Grid-Connected Induction Generator under Naturally Commutated AC Voltage Controller*

[49] Ulrich Kogelschatz1 *Dielectric-barrier Discharges: Their History, Discharge Physics, and Industrial Applications* Plasma Chemistry and Plasma Processing, Vol. 23, No. 1, March 2003

[50] M M Becker, T Hoder, R Brandenburg and D Loffhagen

Analysis of microdischarges in asymmetric dielectric barrier discharges in argon J. Phys. D: Appl. Phys. 46 (2013)

[51] Tagashira H, Sakai Y and Sakamoto S

1977 J. Phys. D: Appl. Phys. 10 1051–63